J Biol Inorg Chem (2016) 21:145–162
DOI 10.1007/s00775-015-1315-x

ORIGINAL PAPER

Investigation of antitumor potential of Ni(II) complexes with tridentate PNO acylhydrazones of 2-(diphenylphosphino) benzaldehyde and monodentate pseudohalides

Božidar Čobeljić[1] · Milica Milenković[1] · Andrej Pevec[2] · Iztok Turel[2] · Miroslava Vujčić[3] · Barbara Janović[3] · Nevenka Gligorijević[4] · Dušan Sladić[1] · Siniša Radulović[4] · Katarina Jovanović[4] · Katarina Anđelković[1]

Received: 15 July 2015 / Accepted: 14 November 2015 / Published online: 26 November 2015

Abstract Square-planar azido Ni(II) complex with condensation product of 2-(diphenylphosphino)benzaldehyde and Girard's T reagent was synthesized and its crystal structure was determined. Cytotoxic activity of the azido complex and previously synthesized isothiocyanato, cyanato and chlorido Ni(II) complexes with this ligand was examined on six tumor cell lines (HeLa, A549, K562, MDA-MB-453, MDA-MB-361 and LS-174) and two normal cell line (MRC-5 and BEAS-2B). All the investigated nickel(II) complexes were cytotoxic against all tumor cell lines. The newly synthesized azido complex showed selectivity to HeLa and A549 tumor cell lines compared to the normal cells (for A549 IC_{50} was similar to that of cisplatin). Azido complex interferes with cell cycle phase distribution of A549 and HeLa cells and possesses nuclease activity towards supercoiled DNA. The observed selectivity of the azido complex for some tumor cell lines can be connected with its strong DNA damaging activity.

Electronic supplementary material The online version of this article (doi:10.1007/s00775-015-1315-x) contains supplementary material, which is available to authorized users.

✉ Katarina Anđelković
kka@chem.bg.ac.rs

[1] Faculty of Chemistry, University of Belgrade, Studentski trg 12-16, 11000 Belgrade, Serbia

[2] Faculty of Chemistry and Chemical Technology, University of Ljubljana, Večna pot 113, 1000 Ljubljana, Slovenia

[3] Institute of Chemistry, Technology and Metallurgy, University of Belgrade, Njegoševa 12, P.O. Box 815, 11000 Belgrade, Serbia

[4] Laboratory for Experimental Pharmacology, Department of Experimental Oncology, Institute for Oncology and Radiology of Serbia, Pasterova 14, Belgrade, Serbia

Keywords Nickel(II) complexes · Girard's T reagent · Phosphine ligands · Cytotoxicity · DNA interactions

Introduction

Hydrazones of 2-(diphenylphosphino)benzaldehyde represent an interesting group of phosphine ligands which possess a combination of soft and hard electron donor atoms and exhibit versatile coordination modes depending on reaction conditions and the nature of central metal ion [1–13]. Of particular importance is the observed biological activity (antimicrobial and antitumor) of these ligands and their complexes [13–21]. Recently, we synthesized two series of square-planar Ni(II) complexes with tridentate PNO acylhydrazones of 2-(diphenylphosphino)benzaldehyde and studied their antimicrobial and antitumor activity [20, 21]. In Ni(II) complexes with the condensation product of 2-(diphenylphosphino)benzaldehyde and ethyl carbazate (**HL1**) (Scheme 1) [20] as well as in Ni(II) complexes with 2-(diphenylphosphino)benzaldehyde 4-phenylsemicarbazone (**HL2**) (Scheme 2) [21] the monoanionic ligand is coordinated through the phosphorus, imine nitrogen and carbonyl oxygen atoms while the fourth coordination place is occupied with one of three different pseudohalides: cyanate, thiocyanate or azide. All Ni(II) complexes with **HL1** ligand showed activity to all investigated tumor cell lines (A549—lung adenocarcinoma cells, MDA-MB-361—breast cancer cell line, HeLa—human cervix carcinoma cells, FemX—melanoma cell line, LS-174—colon cancer cells and K562—human myelogenous leukemia cells) and were more active than the ligand. The azido complex showed activity to K562 leukemia cells of similar intensity as cisplatin and was less cytotoxic to the normal MRC-5 cell line (human fetal lung fibroblast cells) than cisplatin.

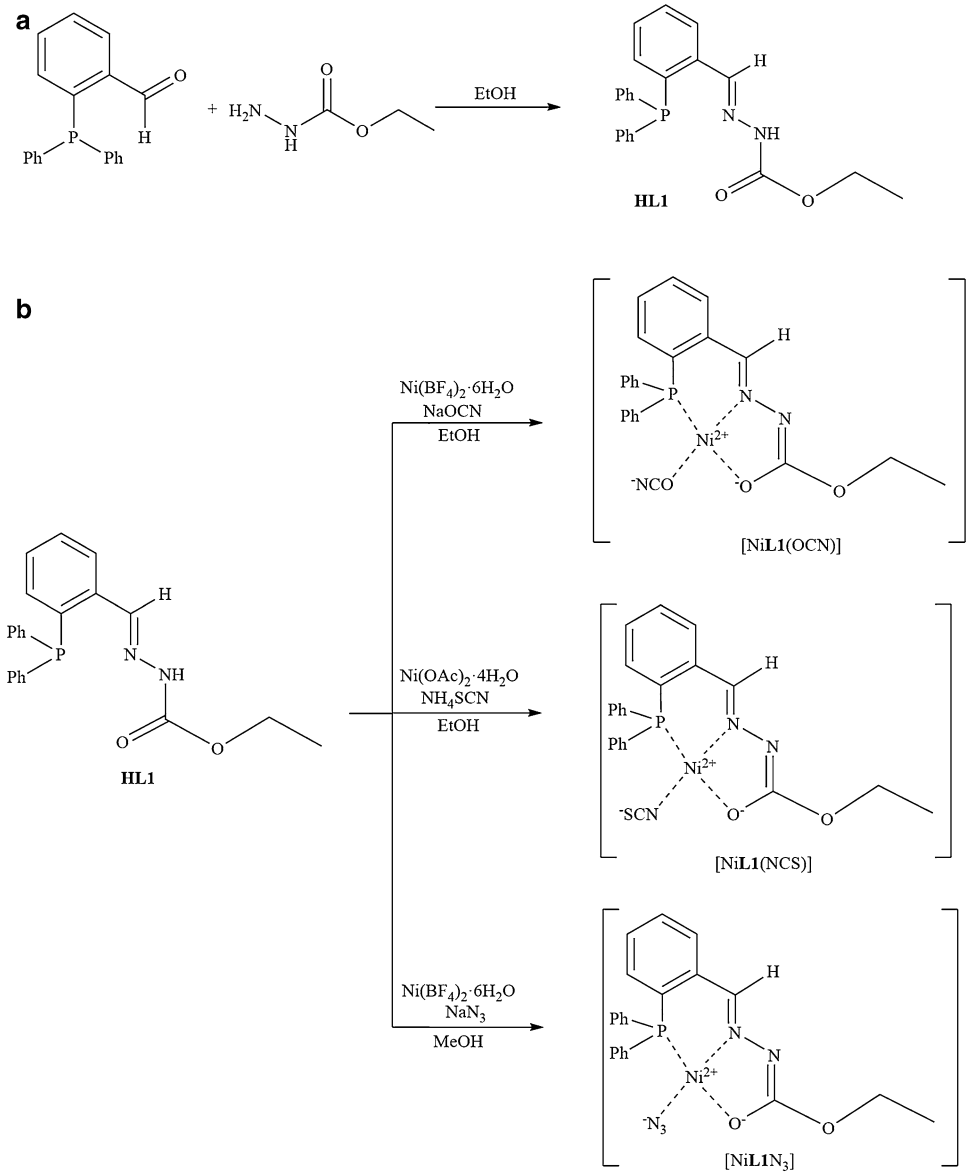

Scheme 1 Synthesis of condensation product of 2-(diphenylphosphino)benzaldehyde and ethyl carbazate (**HL1**) (**a**) and its Ni(II) complexes (**b**)

All Ni(II) complexes exhibited higher cytotoxicity to K562 cells than to other cell lines. The most cytotoxic complex to K562 and MDA-MB-361 cells was the azido complex, to LS-174 cell line the isothiocyanato complex, and to the normal MRC-5 cells the cyanato complex, while there was no significant difference in cytotoxic activity between the complexes to the other investigated cell lines. Complexes of Ni(II) with **HL1** interfered with the cell cycle of tumor cells and induced plasmid DNA cleavage [20]. All Ni(II) complexes with **HL2** ligand showed moderate to strong activity to all investigated tumor cell lines (HeLa, FemX, A549, LS-174, MDA-MB-453 and K562). Azido complex and **HL2** ligand induced perturbation in cell cycle progression (arrest in the S phase, decrease of percentage of cells in G1 phase and no significant increase of apoptotic fraction of cells) [21]. The observed cytotoxicity of azido complex is a consequence of DNA damaging. Previously synthesized octahedral and square-planar Ni(II) complexes with the condensation product of 2-(diphenylphosphino) benzaldehyde and Girard's T reagent (**HL**Cl) and different monodentates, i.e., chloride, cyanate and thiocyanate [22] (Scheme 3), showed a moderate antibacterial activity not only against laboratory control strains but also on clinical isolates of *E. coli* and *P. aeruginosa* strains which were resistant to most of the clinically used antibiotics [23].

In this study, the synthesis and characterization of square-planar azido Ni(II) complex with condensation product of 2-(diphenylphosphino)benzaldehyde and Girard's T reagent is described. As a continuation of our previous investigation of biological activity of Ni(II) complexes with acylhydrazones of 2-(diphenylphosphino)benzaldehyde [20–23] cytotoxic activity and DNA damaging

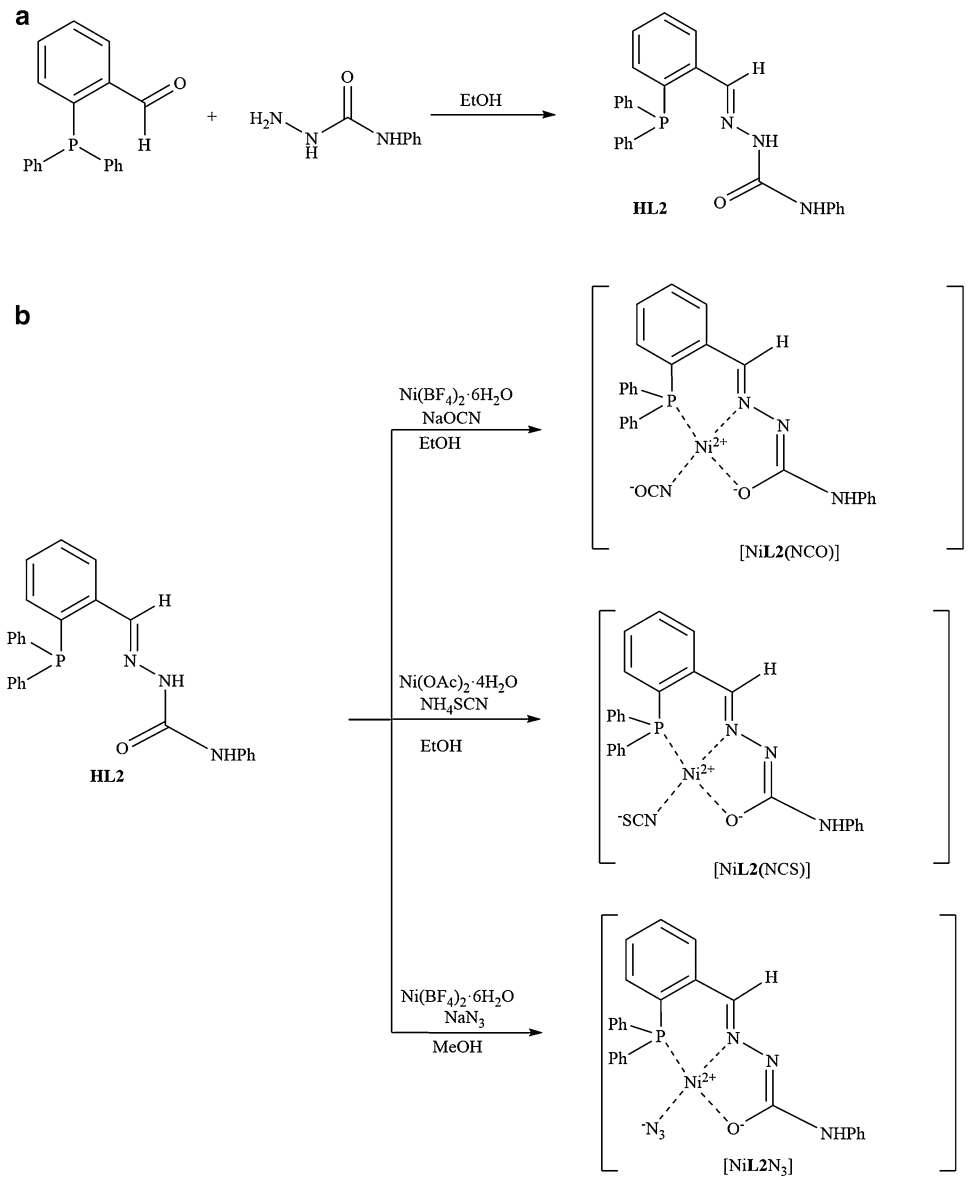

Scheme 2 Synthesis of 2-(diphenylphosphino)benzaldehyde 4-phenylsemicarbazone (**HL2**) (**a**) and its Ni(II) complexes

potential of azido, isothiocyanato, cyanato and chlorido Ni(II) complexes with 2-(diphenylphosphino)benzaldehyde and Girard's T reagent has been examined.

Experimental

Materials and methods

2-(Diphenylphosphino)benzaldehyde (97 %) and Girard's T reagent (99 %) were obtained from Aldrich. IR spectra were recorded on a Perkin–Elmer FT-IR 1725X spectrometer using the ATR technique in the region 4000–400 cm^{-1}. ^{1}H NMR (500 MHz) and ^{13}C NMR (125 MHz) spectra were recorded on a Bruker Avance 500 spectrometer in DMSO–d_6 using TMS as internal standard for ^{1}H and ^{13}C. All spectra were measured at room temperature. UV–Vis spectra were recorded at Shimadzu 1800 UV–Vis spectrometer. Elemental analyses (C, H, N) were performed by standard micro-methods using the ELEMENTARVario ELIII C.H.N.S.O analyzer. Molar conductivity was measured at room temperature (23 °C) on a digital conductivity-meter JENWAY-4009.

Synthesis of HLCl

Ligand **HL**Cl was obtained by condensation reaction of 2-(diphenylphosphino)benzaldehyde and Girard's T reagent using a previously reported method [19]. Yield: 110 mg (47 %) Mp 216 °C. IR (vs-very strong, s-strong, m-medium, w-weak): 3524 (w), 3403 (w), 3308 (w), 3050 (m), 3018 (m), 2970 (m), 2930 (m), 2890 (m), 2817 (w), 1686 (vs),

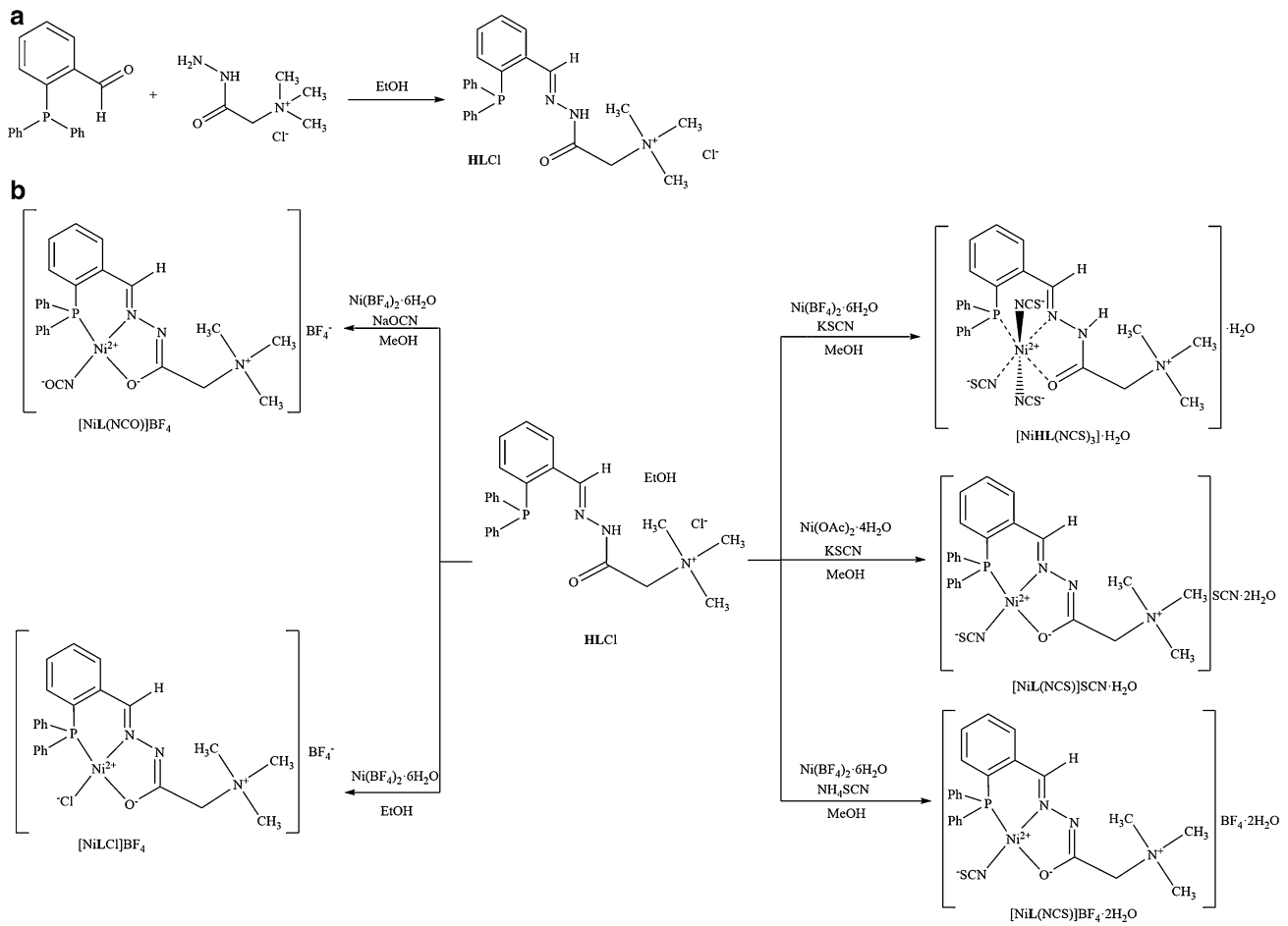

Scheme 3 Synthesis of condensation product of 2-(diphenylphosphino)benzaldehyde and Girard's T reagent (**HL**Cl) (**a**) and its Ni(II) complexes

1657 (m), 1602 (w), 1491 (w), 1475 (s), 1433 (s), 1410 (s), 1342 (w), 1306 (s), 1277 (w), 1212 (w), 1133 (w), 1123 (m), 1095 (w), 1044 (w), 992 (w), 948 (w), 929 (w), 876 (w), 848 (w), 765 (w), 746 (vs), 699 (s), 620 (w), 585 (w), 505 (w), 481 (w), 437 (w). Anal. Calcd. for $C_{24}H_{27}ClN_3O_2P{\cdot}EtOH$ (%): N 8.65, C 64.26, H 6.84. Found: N 8.78, C 64.17, H 6.92. ^{1}H NMR (Chemical shift (ppm), multiplicity, number of H-atoms, coupling constant *J* in Hz): 3.30 (s, 9 H), 4.76 (s, 2 H) 8.79 (d, 1 H, $J = 5.0$ Hz) 6.83 (m, 1H) 7.42 (m, 1 H) 7.49 (m, 1 H) 8.05 (dd, 1 H, $J = 5.0$ Hz) 7.19 (m, 4 H) 7.42 (m, 4 H) 7.42 (m, 2 H) 12.10 (s, 1 H). ^{13}C NMR (chemical shift (ppm), coupling constant *J* in Hz): 53.4, 62.4, 143.4 ($J = 25.0$ Hz), 135.4 ($J = 10$ Hz), 133.2, 130.5, 129.4, 126.3 ($J = 3.75$ Hz), 136.5 ($J = 18.75$ Hz), 137.2 ($J = 18.75$ Hz), 133.5 ($J = 18.75$ Hz), 129.1 ($J = 7.5$ Hz), 129.4, 165.5.

Synthesis of $[NiLN_3]BF_4$

A mixture of 0.08 g (0.23 mmol) $Ni(BF_4)_2{\cdot}6H_2O$ and 0.11 g (0.23 mmol) of **HL**Cl ligand was dissolved in 20 mL methanol and then 0.05 g (0.77 mmol) NaN_3 was added to it. The mixture was refluxed at 72 °C for 2 h. The reaction solution was left to stand at room temperature for 2 days while reddish crystals arose from the solution. Yield 0.10 g (73.6 %). IR: 3309 (w), 3058 (w), 2034 (vs), 1609 (w), 1568 (m), 1482 (w), 1436 (w), 1412 (w), 1330 (w), 1293 (w), 1208 (w), 1086 (s), 1036 (s), 924 (w), 771 (w), 751 (m), 694 (m), 540 (w), 487 (w) (Fig. S1). Elemental analysis calcd for $C_{24}H_{26}BF_4N_6NiOP$: C 48.78 %, H 4.43 %, N 14.22 %, found: C 48.53 %, H 4.64 %, N 14.31 %. Λ_M (1 mM, DMSO): 43.7 Ω^{-1} cm^2 mol^{-1}. λ_{max} (nm) (H_2O): 296, 327, 344, 362, λ_{max} (nm) (DMSO): 298, 326, 344, 362. The same pattern of electronic spectra in DMSO and aqua solution is observed in the case of [Ni**L**(NCS)]BF_4, [Ni**L**(NCS)]SCN, [Ni**L**(NCO)]BF_4 and [Ni**L**Cl]BF_4 complexes. In electronic spectra of square-planar nickel(II) complexes the strong band due to the *d*–*d* electronic transition (dx^2–y^2 ← d*xy*), is observed in the 17,000–22,000 cm^{-1} or 600–450 nm region, while the band observed at higher energies (23,000–30,000 cm^{-1} or

434–333 nm) is a charge transfer band [24]. The mentioned bands related to the *d–d* transition of the Ni(II) square-planar geometry complexes are not observed in visible region, so it is possible that change in the geometry to octahedral occurs, because the characteristic bands in electronic spectra of octahedral Ni(II) complexes are in the Vis–NIR region (25,000–4000 cm^{-1} or 400–250 nm). Additional support for change of geometry in DMSO was obtained by NMR spectrometry, since line broadening and loss of hyperfine splitting occurred in contrast to sharp signals in $CDCl_3$ (for soluble complexes). This indicates the presence of paramagnetic Ni(II) species in DMSO solution.

Synthesis of $[NiHL(NCS)_3]\cdot H_2O$, $[NiL(NCS)]BF_4$, $[NiL(NCS)]SCN$, $[NiL(NCO)]BF_4$ and $[NiLCl]BF_4$

Complexes of Ni(II) with **HL**Cl ligand, $[Ni\mathbf{HL}(NCS)_3]$, $[Ni\mathbf{L}(NCS)]BF_4$, $[Ni\mathbf{L}(NCS)]SCN$, $[Ni\mathbf{L}(NCO)]BF_4$ and $[Ni\mathbf{L}Cl]BF_4$ were synthesized using previously described methods [22, 23].

X-ray structure determination of $[NiLN_3]BF_4$

Crystal data: $C_{24}H_{26}BF_4N_6NiOP$, $M = 591.00$, orthorhombic, space group *Pbca*, $a = 12.5970(7)$ Å, $b = 14.9907(12)$ Å, $c = 27.491(2)$ Å, $V = 5191.4(6)$ $Å^3$, $Z = 8$, $D_c = 1.512$, $\mu = 0.868$ mm^{-1}. A red prism of compound $[Ni\mathbf{L}N_3]BF_4$ with dimensions of 0.20 × 0.02 × 0.02 mm was glued to a glass thread. X-ray intensity data were collected at room temperature with Agilent SuperNova dual source using an Atlas detector and equipped with mirror-monochromated Mo Kα radiation (λ = 0.71073 Å). The data were processed using CRYSALIS PRO [25]. A total of 17,842 reflections were measured, 5952 were independent and 2060 [$I > 2\sigma(I)$] were considered observed. The structures were solved by direct methods using SHELXS-97 [26] and refined with a full-matrix least-squares procedure based on F^2 using SHELXL-97 [26]. All of the non-hydrogen atoms were refined anisotropically. The C6 bonded hydrogen atom was located in a difference map and refined with the distance restraints (DFIX) with C–H = 0.98 and with $U_{iso}(H) = 1.2U_{eq}(C)$. All other C-H hydrogen atoms were included in the model at geometrically calculated positions and refined using a riding model. The final R indices $R_1 = 0.0682$ [$I > 2\sigma(I)$] and $wR_2 = 0.1314$ (all data) were found.

CCDC 1,409,081 contains the supplementary crystallographic data for $[Ni\mathbf{L}N_3]BF_4$. These data can be obtained free of charge from The Cambridge Crystallographic Data Centre via http://www.ccdc.cam.ac.uk/data_request/cif.

Cell culture

Human cervix carcinoma cells (HeLa), lung adenocarcinoma cells (A549), colon cancer cells (LS-174), breast cancer cell lines (MDA-MB-453 and MDA-MB-361), human bronchial epithelial cells (BEAS-2B) and human fetal lung fibroblast cells (MRC-5) cells were maintained as monolayer culture in the Roswell Park Memorial Institute (RPMI) 1640 nutrient medium (Sigma Chemicals Co, USA). Human myelogenous leukemia cells (K562) were maintained in suspension culture. RPMI 1640 nutrient medium was prepared in sterile ionized water, supplemented with penicillin (192 U/mL), streptomycin (200 µg/mL), 4-(2-hydroxyethyl)piperazine-1-ethanesulfonic acid (HEPES) (25 mM), L-glutamine (3 mM) and 10 % of heat-inactivated fetal calf serum (FCS) (pH 7.2). The cells were grown at 37 °C in 5 % CO_2 and humidified air atmosphere, by twice weekly subculture.

Determination of cell survival (MTT assay)

Cytotoxicity of the investigated nickel(II) complexes, the appropriate ligand, nickel(II) salt and salts of corresponding monodentates in comparison to cisplatin, was determined using the 3-(4,5-dimethylthiazol-2yl)-2,5-diphenyltetrazolium bromide (MTT, Sigma-Aldrich) assay. The MTT colorimetric assay is based on the measurement of mitochondrial enzyme succinate dehydrogenase activity, as an indication of cell viability [27]. Cells were seeded in 96-well cell culture plates (NUNC): HeLa (4000 c/w), A549 (6000 c/w), LS-174 (7000 c/w), MDA-MB-453 (5000 c/w), MDA-MB-361 (7000 c/w), BEAS-2B (7000 c/w) and MRC-5 (5000 c/w) in culture medium and grown for 24 h. K562 (6000 c/w) cells were seeded 2 h before treatment. Stock solutions of investigated agents were made in DMSO at concentration of 10 mM, and afterwards diluted with nutrient medium to desired final concentrations (in range up to 100 µM). Cisplatin (CDDP) stock solution was made in 0.9 % NaCl at concentration of 1.66 mM and afterwards diluted with nutrient medium to desired final concentrations (in range up to 100 µM). The final concentration of DMSO per well did not exceed 1 %. Solutions of various concentrations of examined compounds were added to the wells, except the control wells where only nutrient medium was added. All samples were done in triplicate. Nutrient medium with corresponding agent concentrations but without target cells was used as a blank, also in triplicate.

Cells were incubated for 48 h with the test compounds at 37 °C, with 5 % CO_2 in humidified atmosphere. After incubation, 10 µL of MTT solution, 5 mg/mL in phosphate buffer solution (PBS), pH 7.2, was added to each well. Samples were incubated for 4 h at 37 °C with 5 % CO_2 in humidified atmosphere. Formazan crystals were dissolved in 100 µL 10 % sodium dodecyl sulfate (SDS). Absorbance was recorded on the ThermoLabsystems 408 Multiskan EX 200–240 V after 24 h at a wavelength of 570 nm.

Concentration IC_{50} (μM) was defined as the concentration of drug producing 50 % inhibition of cell survival. It is determined from the cell survival diagrams.

Cell cycle analysis

Flow cytometric analysis of cell cycle phase distribution of A549 and HeLa cells, treated with nickel(II) complexes and cisplatin as reference compound was performed after staining fixed cells with propidium iodide (PI) [28]. Cells were seeded at density of 2.5×10^5 cells/well at 6-well plate (NUNC) and grown in nutrition medium. After 24 h A549 cells were continually exposed to [Ni**L**N_3]BF_4, [Ni**L**(NCS)]BF_4 and [Ni**L**Cl]BF_4 complexes with concentrations that correspond to $0.5 \times IC_{50}$ and IC_{50} (determined for 48 h treatment), while HeLa cells were treated with [Ni**L**(NCS)]BF_4, [Ni**L**N_3]BF_4 [Ni**L**(NCO)]BF_4 and [Ni**L**Cl]BF_4 complexes (40 μM) and cisplatin (5 μM). After 24 and 48 h of continual treatment, cells were collected by trypsinization, washed twice with ice-cold PBS, and fixed for 30 min in 70 % EtOH. After fixation, cells were washed again with PBS, and incubated with RNaseA (1 mg/mL) for 30 min at 37 °C. Cells were than stained with PI (400 μg/mL) 15 min before flow cytometric analysis. Cell cycle phase distribution were analyzed using a fluorescence activated sorting cells (FASC) Calibur Becton-Dickinson flow cytometer and Cell Quest computer software.

Fluorescence microscopy analysis of cell death (AO/EB staining)

To examine the mode of HeLa and A549 cell death induced by the investigated nickel(II) complexes, morphological analysis by microscopic examination of acridine orange/ethidium bromide-stained target cells was performed. A549 and HeLa cells were seeded overnight on cover slips in 6-well plates (2×10^5 cells per well) in 2 mL of complete nutrient medium. After 24 h, HeLa cells were treated with [Ni**L**(NCS)]BF_4, [Ni**L**N_3]BF_4, [Ni**L**(NCO)]BF_4, [Ni**L**Cl]BF_4 complexes (in 40 μM concentrations) and CDDP (in 5 μM concentration) for 48 h, while A549 cells were exposed to $0.5 \times IC_{50}$ concentrations of ([Ni**L**(NCS)]BF_4, [Ni**L**N_3]BF_4, [Ni**L**Cl]BF_4) complexes for 48 h. After this period, the target cells were stained with 10 μL of a mixture of the DNA dyes acridine orange (AO) and ethidium bromide (EB) (3 mg/mL AO and 10 mg/mL EB in PBS), and visualized under a fluorescence microscope—Carl Zeiss PALM MicroBeam with Axio Observer.Z1 using AxioCamMRm (filters Alexa Fluor 489 and Alexa Fluor 546) using the LD Plan-NeoFluar 40 ×/0.60 objective. Images were obtained with multidimensional acquisition using digital imaging software (AxioVision Version 4.7; Carl Zeiss Imaging Solutions).

Apoptotic assay

Flow cytometric analysis of cell death induced by investigated nickel(II) complexes ([Ni**L**(NCS)]BF_4, [Ni**L**N_3]BF_4, [Ni**L**(NCO)]BF_4, [Ni**L**Cl]BF_4) and cisplatin as reference compound, was performed by Annexin V-FITC apoptosis detection kit, according to the manufacturer's instructions (BD Biosciences Cat. No. 65874x, Pharmingen San Diego, CA, USA). HeLa cells (2×10^5) were seeded into 6-well plates (Thermo Scientific Nunc™), in 2 mL of RPMI medium. After 24 h of growth, cells were treated with complexes ([Ni**L**(NCS)]BF_4, [Ni**L**N_3]BF_4, [Ni**L**(NCO)]BF_4, [Ni**L**Cl]BF_4) or cisplatin, for 48 h, at 40 μM concentration for nickel complexes and 5 μM concentration for cisplatin. After treatment, cells were washed with ice-cold PBS and then resuspended in 200 μL binding buffer (10 mM HEPES/NaOH pH 7.4, 140 mM NaCl, 2.5 mM $CaCl_2$). 100 μL of cell suspension (10^5 cells) was transferred to a 5-mL culture tube and mixed with 5 μL of Annexin V-FITC and 5 μL of propidium iodide (PI). After incubation for 15 min, at 25 °C in the dark, 400 μL of binding buffer was added to each tube and analyzed using a FACS Calibur Becton-Dickinson flow cytometer and Cell Quest computer software. A minimum of 10,000 cells were analyzed per sample.

DNA binding experiments

Calf thymus DNA (lyophilized, highly polymerized, obtained from Serva, Heidelberg) (CT-DNA) was dissolved in Tris buffer (10 mM Tris–HCl, pH 7.9) overnight at 4 °C. This stock solution was stored at 4 °C and was stable for several days. A solution of CT-DNA in water gave a ratio of UV absorbance at 260 and 280 nm, A_{260}/A_{280} of 1.89–2.01, indicating that DNA was sufficiently free of protein. The concentration of DNA (2.86 mg/mL) was determined from the UV absorbance at 260 nm using the extinction coefficient $\varepsilon_{260} = 6600\ M^{-1}\ cm^{-1}$ [29]. The Ni(II) complexes ([Ni**L**N_3]BF_4, [Ni**L**(NCS)]BF_4 and [Ni**L**Cl]BF_4) were dissolved in dimethyl sulfoxide in concentrations of 10 mM. These solutions were used as stock solutions.

UV–visible measurements

For a UV–Vis measurement, to DNA solution (10 μL of CT-DNA) was added a small volume of a stock solution of Ni(II) complex (final concentration 30, 50 or 70 μM) and the volume was adjusted up to 1 mL with 40 mM bicarbonate buffer, pH 8.4. Reaction mixtures were incubated at 37 °C for 90 min with occasional vortexing. UV–vis spectra were recorded on a UV-1800 Shimadzu UV/Visible spectrophotometer operating from 200 to 800 nm in 1.0 cm quartz cells. Spectra of Ni(II) complexes of the

same concentrations were also recorded, as well as spectra of CT-DNA.

Fluorescence measurements

The competitive interactions of Ni(II) complexes and the fluorescence probe, either ethidium bromide (EB) or Hoechst 33258 (H), with CT-DNA have been studied by measuring the change of fluorescence intensity of the probe–DNA solution after addition of the complex. Reaction mixtures containing 100 μM of CT-DNA (calculated per phosphate) in 1 mL of 40 mM bicarbonate solution (pH 8.4) were pretreated with 1.5 μL of 1 % H probe solution (28 μM final concentration) or 1 μL of 1 % EB solution (25 μM final concentration) (in separate experiments) for 20 min and the mixture was analyzed by fluorescence measurement. Then the increasing concentrations (0.5, 1, 1.5, 2, 4, 6, 8, 10, 12, 14, 16, 18 and 20 μM) of the complex were successively added and the change in the fluorescence intensity was measured using a Thermo Scientific Lumina Fluorescence spectrometer (Finland) equipped with a 150 W Xenon lamp. The slits on the excitation and emission beams were fixed at 10 nm. All measurements were performed by excitation at 350 nm for Hoechst 33258, and by excitation at 500 nm for EB in the range of 390–600 nm. The control was probe–CT-DNA solution. Complexes $[Ni\mathbf{L}(NCS)]BF_4$, $[Ni\mathbf{L}Cl]BF_4$ and $[Ni\mathbf{L}N_3]BF_4$ did not have fluorescence under applied conditions. The obtained fluorescence quenching data were analyzed according to the Stern–Volmer equation [30]:

$$I_0/I = 1 + \mathrm{Kr} \quad (1)$$

where I_0 and I represent the fluorescence intensities of probe–CT-DNA in absence and presence of the Ni(II)complex, respectively, K is the quenching constant. The K value is calculated from the ratio of the slope to the intercept from the plot of I_0/I versus $r(r = \left[\mathrm{Ni(II)complex}\right]/[\mathrm{CT-DNA}]$.

Primary spectra of all spectrometric measurements were imported into OriginPro 8.0 and were processed by this software package.

DNA cleavage experiments

For DNA cleavage experiments the plasmid pUC19 (2686 bp, purchased from Sigma-Aldrich, USA) was prepared by its transformation in chemically competent cells *Escherichia coli* strain XL1 blue. Amplification of the clone was done according to the protocol for growing *E. coli* culture overnight in LB medium at 37 °C [31] and purification was performed using Qiagen Plasmid plus Maxi kit. Finally, DNA was eluted in 10 mM Tris–HCl buffer and stored at −20 °C. The concentration of plasmid DNA (512 ng/μL) was determined by measuring the absorbance of the DNA-containing solution at 260 nm. One optical unit corresponds to 50 μg/mL of double-stranded DNA.

The cleavage reaction of supercoiled pUC19 DNA with different concentration of ($[Ni\mathbf{L}N_3]BF_4$, $[Ni\mathbf{L}(NCS)]BF_4$ and $[Ni\mathbf{L}Cl]BF_4$) was investigated by incubation of 512 ng of plasmid in a 20 μL reaction mixture in 40 mM bicarbonate buffer (pH 8.4) at 37 °C, for 90 min. The reaction mixtures were vortexed from time to time. The reaction was terminated by short centrifugation at 10,000 rpm and addition of 5 μL of loading buffer (0.25 % bromophenol blue, 0.25 % xylene cyanol FF and 30 % glycerol in TAE buffer, pH 8.24 (40 mM Tris–acetate, 1 mM EDTA)).

Digestion of plasmid pUC19 DNA by restriction enzymes

Enzyme digestions were carried out by incubating the untreated and $[Ni\mathbf{L}N_3]BF_4$, $[Ni\mathbf{L}(NCS)]BF_4$ and $[Ni\mathbf{L}Cl]BF_4$ treated pUC19 plasmid samples with the restriction endonucleases *Bam*HI or *Hin*dIII (Sigma, USA). 512 ng of plasmid DNA treated or untreated with 1 μL of 10 mM Ni(II) complex were incubated with 1 μL (10 U) of the restriction endonucleases at 37 °C for 9 h or 16 h in 20 μL of the digestion buffer (10 mM Tris–HCl, pH 8.0, containing 100 mM NaCl, 5 mM $MgCl_2$, 1 mM 2-mercaptoethanol). The samples were then analyzed by agarose gel electrophoresis. In the second set of experiments, plasmid samples were first treated with Ni(II) complexes, and the obtained products were subsequently treated with the restriction nucleases.

Agarose electrophoresis

The samples were subjected to electrophoresis on 1 % agarose gel (Amersham Pharmacia-Biotech, Inc) prepared in TAE buffer pH 8.24. The electrophoresis was performed at a constant voltage (80 V) until bromophenol blue had passed through 75 % of the gel. A Submarine Mini-gel Electrophoresis Unit (Hoeffer HE 33) with an EPS 300 power supply was used. After electrophoresis, the gel was stained for 30 min by soaking it in an aqueous ethidium bromide solution (0.5 μg mL^{-1}). The stained gel was illuminated under a UV transilluminator Vilber-Lourmat (France) at 312 nm and photographed with a Nikon Coolpix P340 Digital Camera through filter DEEP YELLOW 15 (TIFFEN, USA).

Phosphatase activity

Phosphatase activity of the complexes was measured using disodium *p*-nitrophenyl phosphate hexahydrate (pNPP)

Scheme 4 Synthesis of $[NiLN_3]BF_4$ complex

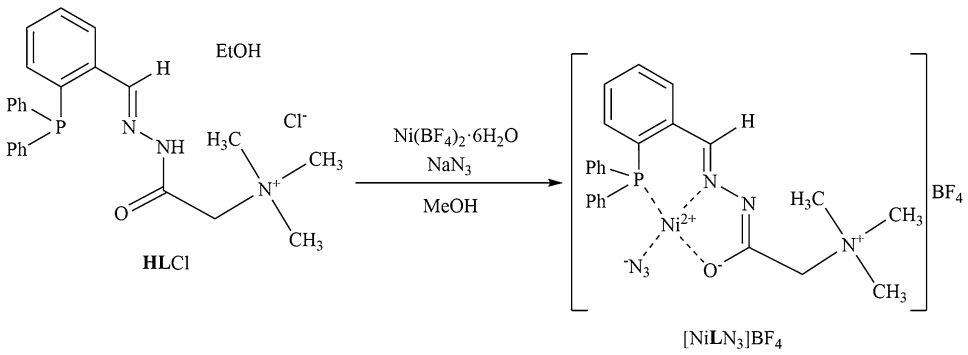

according the literature [32]. The solvent chosen for this study was 97.5 % DMSO. Solution of substrate and $[NiLN_3]BF_4$, $[NiL(NCS)]BF_4$ and $[NiLCl]BF_4$ complexes were freshly prepared and all spectra were recorded for 2 h from solution containing 1 mmol of the substrate and 0.05 mmol of the Ni(II) complexes in 1 mL of solution.

Results and discussion

Synthesis

Ligand **HL**Cl was obtained by condensation reaction of 2-(diphenylphosphino)benzaldehyde and Girard's T reagent [19]. Complexes of Ni(II) with condensation product of 2-(diphenylphosphino)benzaldehyde and Girard's T reagent $[NiHL(NCS)_3]$, $[NiL(NCS)]BF_4$, $[NiL(NCS)]SCN$, $[NiL(NCO)]BF_4$ and $[NiLCl]BF_4$ were synthesized using previously described methods [22, 23].

In the reaction of $Ni(BF_4)_2{\cdot}6H_2O$ and NaN_3 with **HL**Cl ligand in methanol $[NiLN_3]BF_4$ complex was obtained (Scheme 4). Square-planar surroundings of Ni(II) ion consist of the acylhydrazone ligand, in deprotonated zwitterionic form, coordinated as a tridentate through phosphorus, imine nitrogen and carbonyl oxygen atoms and azido ligand in the fourth coordination place.

IR spectra

In the IR spectrum of $[NiLN_3]BF_4$ complex a new band corresponding to $\nu(^-O–C=N)$ of the deprotonated hydrazide moiety appeared at 1568 cm^{-1}, instead of the carbonyl band from the uncoordinated ligand at 1686 cm^{-1}. Coordination of azomethine nitrogen atom resulted in bathochromic shift of $\nu(C=N)$ vibration from 1657 cm^{-1} in the spectrum of **HL**Cl to 1609 cm^{-1} in the spectrum of $[NiLN_3]BF_4$ complex. A band at 2033 cm^{-1} in the spectrum of $[NiLN_3]BF_4$ complex originates from the coordinated azido ligand. A band originating from tetrafluoroborate anion in the outer sphere of the complex is located at 1036 cm^{-1} [33, 34].

X-ray crystallographic analysis

The nickel complex $[NiLN_3]BF_4$ crystallized in orthorhombic crystal system with space group *Pbca*. ORTEP presentation of the structure is given in Fig. 1, while bond lengths and angles are listed in Table 1. The complex cation in $[NiLN_3]BF_4$ consists of one tridentate molecule of deprotonated PNO ligand coordinated to the Ni(II) ion and coordinated azide anion forming a square-planar geometry around Ni(II) ion. BF_4^- ion acts as counterion in the crystal structure complex. Bond distances and angles in

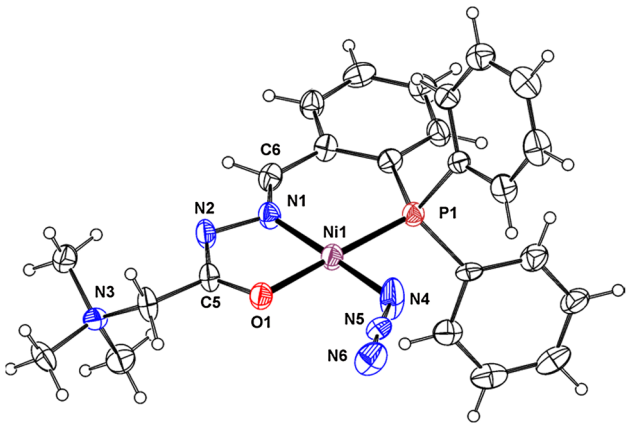

Fig. 1 ORTEP plot of $[NiLN_3]BF_4$ from the X–ray crystal structure with thermal ellipsoids at 30 % probability for non-H atoms and *open circles* for H-atoms. BF_4^- is omitted for the reason of clarity

Table 1 Selected bond lengths (Å) and angles (°) for $[NiLN_3]BF_4$

Ni1–N1	1.859 (4)	P1–Ni1–N1	95.82 (14)
Ni1–N4	1.867 (5)	P1–Ni1–N4	86.56 (17)
Ni1–O1	1.888 (4)	P1–Ni1–O1	178.96 (15)
Ni1–P1	2.1478 (16)	N1–Ni1–N4	177.2 (2)
N1–N2	1.422 (5)	N1–Ni1–O1	84.57 (18)
N1–C6	1.270 (7)	N4–Ni1–O1	93.1 (2)
N2–C5	1.312 (7)	Ni1–N1–N2	112.1 (3)
O1–C5	1.262 (6)	N1–N2–C5	108.8 (4)

compound [Ni**L**N_3]BF_4 are in accordance with the reported values for the similar square-planar complexes where linear thiocyanate [22], isocyanate [21], or azide [11, 20, 21] anion is coordinated through nitrogen atom to the Ni metal center. The sum of the nickel-containing angles in complex [Ni**L**N_3]BF_4 is 360°. The position of the Ni(II) ion is 0.0035(27) out of the best plane that contained the coordination sphere of four atoms. H-bonds between BF_4^- and the complex ion C–H···F, as well as between two complex ions C14–H14···N6 are weak and do not play an important role in the crystal structure of [Ni**L**N_3]BF_4 complex (Table S1).

Determination of cell survival (MTT assay)

Cytotoxic activity of the investigated nickel(II) complexes and cisplatin (CDDP) as standard cytotoxic agent was determined by MTT assay after 48 h treatment of six tumor cell lines (HeLa, A549, K562, MDA-MB-453, MDA-MB-361 and LS-174) and two normal cell line (MRC-5 and BEAS-2B). The results are shown in Table 2 in terms of IC_{50} values for 48 h incubation period. IC_{50} values were calculated as mean values obtained from two to three independent experiments and presented with their standard deviations.

Results of this assay indicate that all investigated nickel(II) complexes showed a moderate to strong cytotoxic activity to all tumor cell lines in comparison with cisplatin. Complexes [Ni**L**(NCS)]BF_4, [Ni**L**N_3]BF_4 and [Ni**L**Cl]BF_4 have shown a more prominent antiproliferative activity in A549 cells, even stronger than cisplatin, which is worth mentioning, because of lower sensitivity of A549 cell line to treatments in general. Nevertheless, the newly synthesized azido complex showed selectivity to two tumor cell lines (HeLa and A549) compared to the normal cells (for A549 IC_{50} was similar to that of cisplatin). The best cytotoxic activity was observed on K562, A549 and MDA-MB-361 cell lines for [Ni**L**(NCS)]BF_4 and for [Ni**HL**$(NCS)_3$] on LS-174 cell line.

The ligand itself (**HL**Cl) did not exhibit as strong cytotoxic effect against tumor cells as nickel(II) complexes, which leads to conclusion that metal–ligand complexation is crucial for cytotoxic properties of the compounds. The examined nickel(II) salt and salts of corresponding monodentates after 48 h of incubation did not reach IC_{50} values in the range of applied concentrations (up to 100 μM) in all investigated cell lines.

Comparison of cytotoxic activity of Ni(II) complexes with **HL**Cl ligand with the activity of the two previously synthesized series of Ni(II) complexes with **HL1** [20] and **HL2** [21] ligands indicates that the nature of the hydrazone ligand and monodentates has important influence on cytotoxicity of the complexes (Table 3).

The observed trend of cytotoxicity of hydrazone ligands on normal MRC-5 cell line was **HL1** < **HL**Cl < **HL2**. Comparison of toxicity of Ni(II) complexes with 2-(diphenylphosphino)benzaldehyde acylhydrazones (**HL**Cl, **HL1** and **HL2**) and different pseudohalogenides with cisplatin toxicity on MRC-5 cell line is presented in Table 4 [20, 21].

Having in mind the results of cytotoxic activity of investigated Ni(II) complexes it is clear that their activity depends on the synergistic effect of 2-(diphenylphosphino) benzaldehyde acylhydrazones, monodentate ligand at the remaining coordination site and anions in the case of electrolyte complexes. Different activity of [Ni**L**(NCS)]BF_4 and [Ni**L**(NCS)]SCN is the consequence of differences in

Table 2 Results of MTT assay presented as IC_{50} (μM) values obtained after 48-h treatment

	HeLa	K562	A549	LS-174	MDA-MB-361	MDA-MB-453	MRC-5	BEAS-2B
HLCl	51.25 ± 2.98	86.88 ± 2.92	71.13 ± 3.04	>100	>100	>100	45.40 ± 1.16	n.t.
[Ni**HL**$(NCS)_3$]	34.22 ± 3.80	52.10 ± 16.40	72.20 ± 0.17	35.62 ± 1.18	40.99 ± 0.19	48.18 ± 0.83	18.96 ± 0.90	n.t.
[Ni**L**(NCS)]BF_4	28.59 ± 4.12	25.16 ± 3.61	14.62 ± 2.99	>100	19.62 ± 3.31	46.34 ± 3.58	19.61 ± 4.26	55.12 ± 7.68
[Ni**L**(NCS)]SCN	25.87 ± 4.16	76.27 ± 6.84	50.80 ± 12.08	97.28 ± 1.53	36.64 ± 3.95	44.31 ± 2.12	25.54 ± 0.53	n.t.
[Ni**L**N_3]BF_4	22.18 ± 2.04	63.18 ± 6.63	22.98 ± 2.13	70.39 ± 4.24	39.39 ± 4.37	49.74 ± 0.23	32.00 ± 0.84	49.11 ± 0.56
[Ni**L**(NCO)]BF_4	24.29 ± 0.97	68.99 ± 5.97	57.62 ± 3.85	78.94 ± 3.69	33.54 ± 3.88	45.60 ± 4.84	15.58 ± 5.64	47.63 ± 13.44
[Ni**L**Cl]BF_4	24.25 ± 0.44	50.17 ± 2.59	14.94 ± 3.78	>100	27.22 ± 7.34	72.01 ± 4.08	16.33 ± 3.63	48.57 ± 6.84
$Ni(BF_4)_2{\cdot}6H_2O$	>100	>100	>100	>100	>100	>100	>100	n.t.
NaOCN	>100	>100	>100	>100	>100	>100	>100	n.t.
KSCN	>100	>100	>100	>100	>100	>100	>100	n.t.
NaN_3	>100	>100	>100	>100	>100	>100	>100	n.t.
CDDP	5.17 ± 0.29	18.56 ± 3.28	26.21 ± 5.36	22.41 ± 7.18	14.7 ± 1.2	13.51 ± 2.56	12.13 ± 0.92	14.19 ± 1.43

IC_{50} values were calculated as mean values obtained from two to three independent experiments and presented with their standard deviations. A sign (>) indicates that IC_{50} value is not reached in the examined range of concentrations (the sign is in front of the maximum value of the concentration in the examined range of concentrations).n.t.-not tested

Table 3 Selectivity of Ni(II) complexes with 2-(diphenylphosphino) benzaldehyde acylhydrazones (**HL**Cl, **HL1** and **HL2**) and different pseudohalogenides towards investigated tumor cell lines (HeLa, K562, A549, LS-174, MDA-MB-361, MDA-MB-453)

X = pseudohalogenide	[Ni**L**X]	[Ni**L1**X]	[Ni**L2**X]
OCN^-	LS-174 MDA-MB-361	K562	A549 HeLa MDA-MB-453
SCN^-	K562 A549 MDA-MB-361	LS-174	HeLa MDA-MB-453
N_3^-	A549	K562 MDA-MB-361	HeLa LS-174 MDA-MB-453

Table 4 Toxicity of Ni(II) complexes with 2-(diphenylphosphino) benzaldehyde acylhydrazones (**HL**Cl, **HL1** and **HL2**) and different pseudohalogenides on MRC-5 cell line

X = pseudohalogenide	[Ni**L**X]	[Ni**L1**X]	[Ni**L2**X]
OCN^-	++	++	+++
SCN^-	++	+	+++
N_3^-	+	+	+++

(+++ stronger, ++ similar, + lower toxicity of Ni(II) complex in comparison with cisplatin)

coordination properties of corresponding anions as well as the possibility of thiocyanate oxidation in biological systems. Biological activity of OCN^-, SCN^- and N_3^- was described in the literature [35–37]. So the possible role of investigated Ni(II) complexes is the transport of biologically active pseudohalogenides into the cell. Also, phosphine acylhydrazone ligands are biologically active compounds and coordination of metal ion to the phosphorus atom can prevent oxidation of phosphine to phosphine oxide and as a consequence of this enhance biological activity [38].

Cell cycle analysis

Cell cycle analysis of A549 cells treated with nickel(II) complexes ([Ni**L**N_3]BF_4, [Ni**L**(NCS)]BF_4 and [Ni**L**Cl]BF_4) and cisplatin was performed by flow cytometry after staining with propidium iodide [28]. Cells were continually exposed to nickel(II) complexes ([Ni**L**N_3]BF_4, [Ni**L**(NCS)]BF_4 and [Ni**L**Cl]BF_4) and cisplatin for 24 and 48 h with increasing concentrations of agents (0.5 × IC50 and IC50). After 24 h of continual treatment with complexes [Ni**L**N_3]BF_4, [Ni**L**(NCS)]BF_4 and [Ni**L**Cl]BF_4, increase of apoptotic fraction of cells (Sub-G1 fraction) was noted (Fig. 2). This increase was not concentration-dependent because doubling the concentration of active substance does not change the percentage of dead cells. At the same incubation period decrease in G2 fraction of A549 cells was also noted. Only in the case of [Ni**L**N_3]BF_4 complex decrease in the percentage of cells in S phase of cell cycle was observed. After 48 h of incubation with complexes [Ni**L**(NCS)]BF_4 and [Ni**L**Cl]BF_4 no changes in cell cycle phase distribution occurred compared to control population of cells. After 48 h of treatment with [Ni**L**N_3]BF_4 complex the increase of G1 and decrease of S phase fraction were observed, while the percentage of cells in sub G1 phase was the same as in the control.

Analysis of perturbations of HeLa cells treated with selected complexes [Ni**L**(NCS)]BF_4, [Ni**L**(N_3)]BF_4, [Ni**L**(NCO)]BF_4 and [Ni**L**Cl]BF_4 (40 μM) and cisplatin (5 μM) after 48 h was also performed. Nickel complexes [Ni**L**(NCS)]BF_4, [Ni**L**N_3]BF_4, [Ni**L**(NCO)]BF_4 and [Ni**L**Cl]BF_4 show slight decrease of percent of cells in G1 phase and increase of percent of cells in S phase (Fig. 3). While cisplatin, as expected according to literature data induced more aggressive perturbations of cell cycle with block of cell cycle in S phase in HeLa cells [21, 39].

Fluorescence microscopy analysis of cell death (AO/EB staining)

In order to assess the apoptotic potential of the investigated nickel(II) complexes ([Ni**L**(NCS)]BF_4, [Ni**L**N_3]BF_4, [Ni**L**(NCO)]BF_4 and [Ni**L**Cl]BF_4), morphological analysis by fluorescence microscopy of acridine orange/ethidium bromide-stained HeLa and A549 cells was performed. Typical morphological features of the apoptotic cells are shrinkage, retraction of pseudopods, reduction of cellular volume (pyknosis), chromatin condensation, nuclear fragmentation, minor modification of cytoplasmic organelles, plasma membrane blebbing [40]. In live cells and in early apoptotic cells, considering that plasma membrane integrity is preserved, only acridine orange enters the cell while ethidium bromide is excluded and the nucleus is stained green. In late apoptosis or necrosis along with the loss of membrane integrity, both dyes enter the cell and the nucleus becomes orange-red.

After 48 h of treatment of HeLa cells with investigated complexes [Ni**L**(NCS)]BF_4, [Ni**L**N_3]BF_4, [Ni**L**(NCO)]BF_4, [Ni**L**Cl]BF_4 (in 40 μM concentrations) and CDDP (in 5 μM concentration) there is a prominent reduction in the number of cells compared to control population, together with initial retracting of pseudopods and rounding off (Fig. 4). However, not all cells become uniformly round, cells with spindle-shaped morphology are still present and majority of cells has intact membrane since they colored green. Different types of alterations were noticed after treatment with complexes [Ni**L**(NCS)]BF_4, [Ni**L**N_3]BF_4

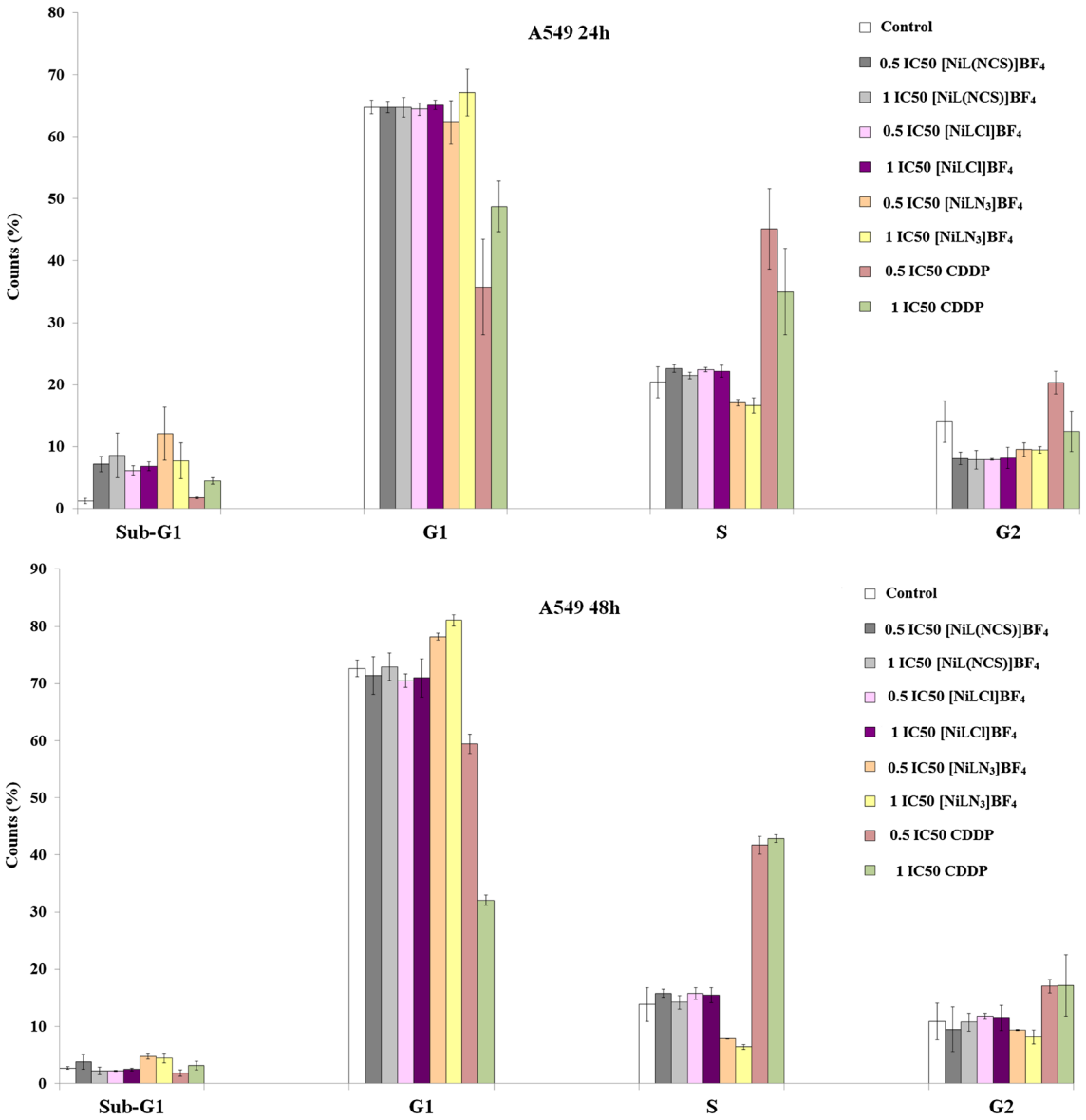

Fig. 2 Effect of the complexes [Ni**L**(NCS)]BF_4, [Ni**L**Cl]BF_4 and cisplatin (CDDP) on cell cycle progression of A549 cells following 24 and 48 h incubation with concentrations of investigated complexes corresponding to 0.5 × IC_{50} and IC_{50}. Controls were untreated cells (incubated with nutrient medium only). The results are expressed as mean ± standard deviations of three independent experiments

and [Ni**L**Cl]BF_4 like chromatin condensation, membrane blebbing and apoptotic bodies characteristic to the various stages of apoptosis. Necrotic cells with red enlarged nucleus without or with low chromatin condensation are also spotted (Fig. 4 [Ni**L**(NCS)]BF_4 and [Ni**L**Cl]BF_4). Complex [Ni**L**(NCO)]BF_4 except the beginning of rounding off have not induced other morphological changes.

Control A549 cells presented on photomicrographs in Fig. S2 are of light green color, short, spindle-shaped and triangle-shaped, with significant growth density. Only after 48 h of continual action with 0.5 × IC_{50} concentrations of investigated nickel(II) complexes ([Ni**L**(NCS)]BF_4, [Ni**L**N_3]BF_4 and [Ni**L**Cl]BF_4) the beginning of nuclear condensation is observed, which is considered to be an early apoptotic marker. However, other characteristic hallmarks of apoptosis, such as membrane blebbing and apoptotic bodies, have not been noticed.

Apoptotic assay

Fluorescent microscopy after AO/EB staining show that complexes [Ni**L**(NCS)]BF_4, [Ni**L**N_3]BF_4 and [Ni**L**Cl]BF_4 after 48 h treatment of HeLa cells have a potential of inducing some apoptotic characteristics of cell death. Further

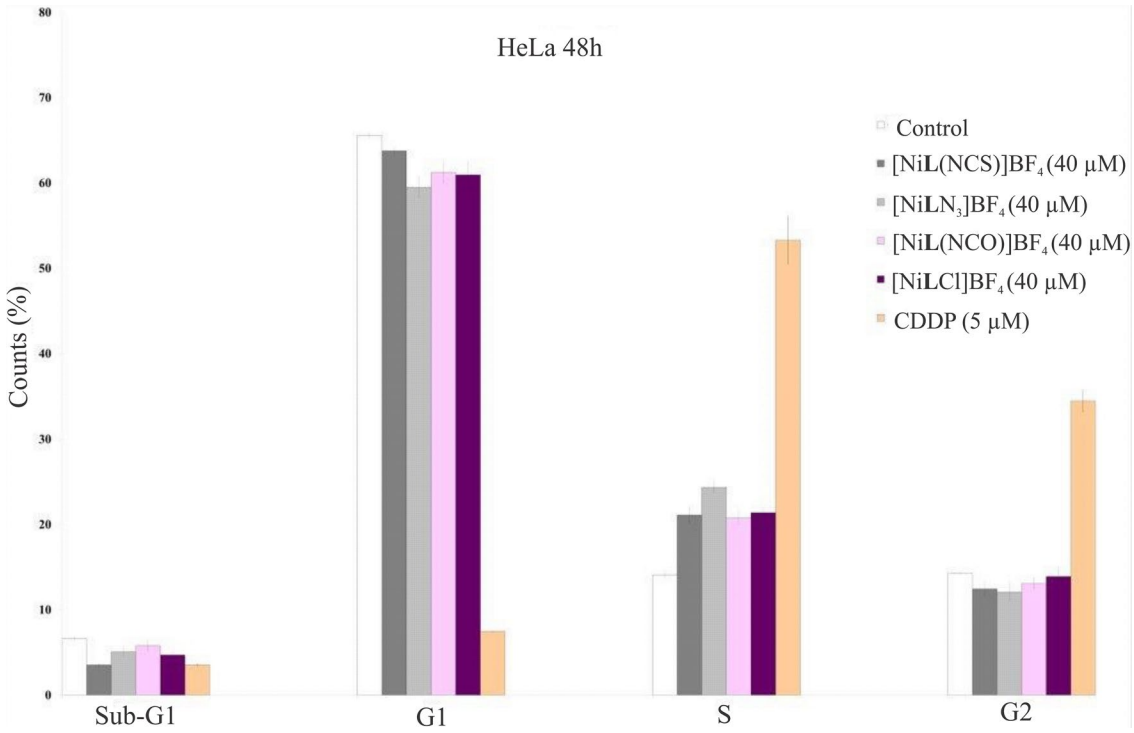

Fig. 3 Effect of the complexes [Ni**L**(NCS)]BF_4, [Ni**L**N_3]BF_4, [Ni**L**(NCO)]BF_4, [Ni**L**Cl]BF_4 and cisplatin (CDDP) on cell cycle progression of HeLa cells after 48 h incubation with 40 μM concentration for nickel(II) complexes and 5 μM concentration for cisplatin. Controls were untreated cells (incubated with nutrient medium only). The results are expressed as mean ± standard deviations of three independent experiments

analysis of their apoptotic potential was investigated using flow cytometry dual staining with Annexin V-FITC and PI, method that enables detection of translocation of phosphatidylserine from the inner to the outer side of plasma membrane during apoptosis. In Fig. S3 representative dot plot diagrams are shown, with percentages of viable cells (Annexin V-FITC and PI negative), early apoptotic cells (Annexin V-FITC positive and PI negative), late apoptotic cells and necrotic cells (Annexin V-FITC negative and PI positive) and dead cells (Annexin V-FITC negative and PI positive). Results shown as bar graph in Fig. 5 indicate that after 48 h treatment and 40 μM concentration of investigated nickel(II) complexes ([Ni**L**(NCS)]BF_4, [Ni**L**N_3]BF_4, [Ni**L**(NCO)]BF_4 and [Ni**L**Cl]BF_4) no increase of percentage of cells labeled with Annexin V-FITC (early apoptotic), nor cells labeled with both dyes Annexin V-FITC and PI (late apoptotic and necrotic cells) compared to control was found. However, number of dead cells increased to 14.83 % for [Ni**L**(NCS)]BF_4, 33.9 % for [Ni**L**N_3]BF_4, 14.285 % for [Ni**L**(NCO)]BF_4 and 20.765 % for [Ni**L**Cl]BF_4).

Lack of compatibility of results of AO/EB staining and fluorescent microscopy analysis and Annexin V-FITC/propidium iodide staining and analysis on flow cytometer lead to the necessity of further research of precise mechanism of action.

DNA binding activity and mode of DNA interaction

The hyperchromism and hypochromism are regarded as spectral evidence for DNA double-helix structural change when DNA reacts with other molecules. The hyperchromism originates from the disruption of the DNA duplex secondary structure and the hypochromism originates from the stabilization of the DNA duplex by either the intercalation binding mode or the electrostatic effect of small molecules [41, 42]. Electronic absorption spectra of the nickel complexes [Ni**L**(NCS)]BF_4, [Ni**L**Cl]BF_4 and [Ni**L**N_3]BF_4 recorded at different concentrations without or with fixed concentration of CT-DNA are shown in Fig. 6a–c. UV–Vis spectra of all three Ni(II) complexes displayed similar absorption bands. It was found that the maximum absorption of the compounds was centered at 294 nm with shoulders at 339–343 and 358–368 nm. Upon interaction of Ni(II) complexes with CT-DNA, the peaks at 294 nm disappeared, while DNA absorption maximum was shifted from 258 to 251 nm, indicating the formation of a [Ni**L**X]BF_4─CT-DNA complex. Detailed absorption changes induced by binding of the Ni(II) complexes to CT-DNA were further calculated, Fig. 6d–f. The absorption value of the sum of absorbances at 258 nm of a free Ni(II) complex

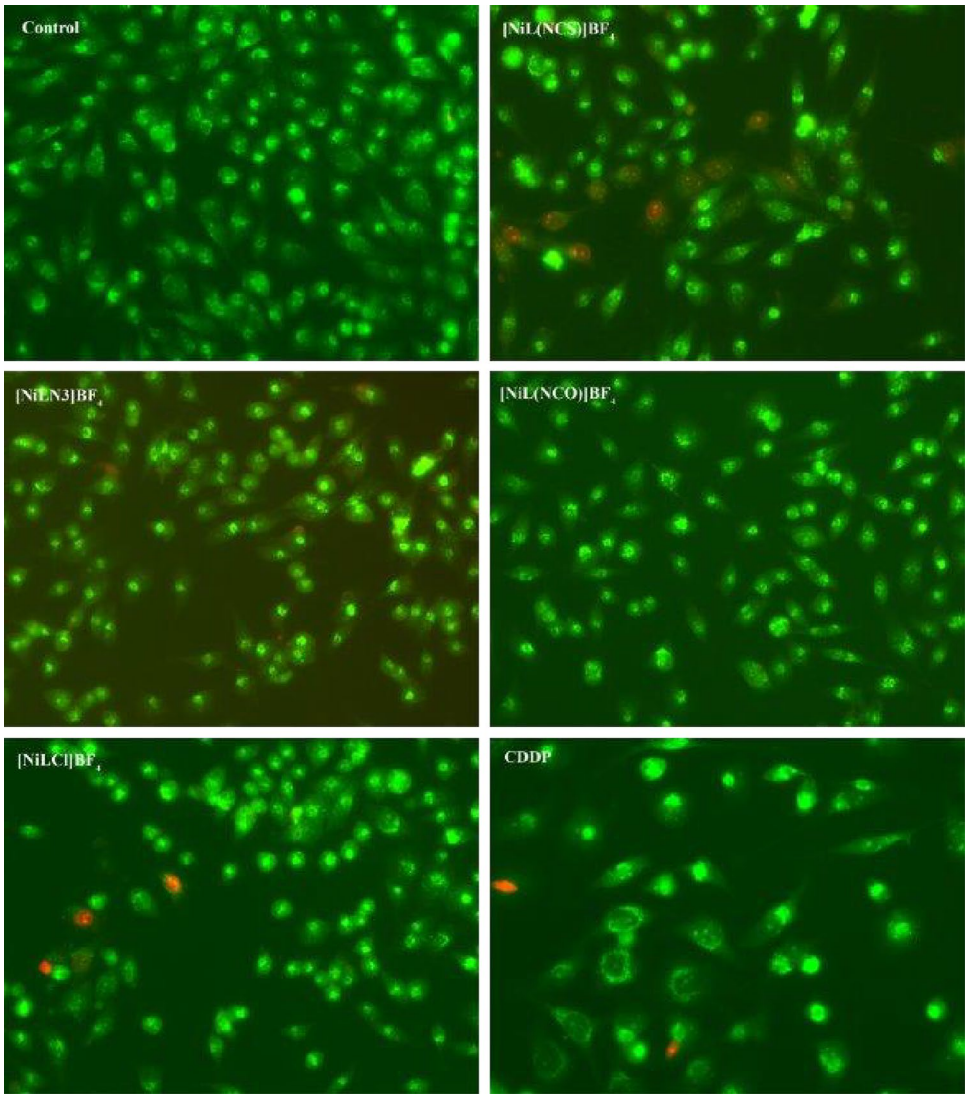

Fig. 4 Photomicrographs of acridine orange/ethidium bromide-stained HeLa cells in control and HeLa cells exposed for 48 h to nickel(II) complexes [Ni**L**(NCS)]BF_4 [Ni**L**N_3]BF_4 [Ni**L**(NCO)]BF_4, [Ni**L**Cl]BF_4 (40 μM concentration) and CDDP (5 μM concentration)

and free CT-DNA was a little different from the absorption value of a [Ni**L**X]BF_4─CT-DNA. The hypochromism of about 7 % has been observed with lower concentrations of [Ni**L**(NCS)]BF_4, Fig. 6d. The similar decrease in absorption intensity at 258 nm has also been observed after interaction of 30 μM [Ni**L**Cl]BF_4 with CT-DNA (the hypochromism was calculated as 9 %), Fig. 6e. The DNA showed the least changes after interaction with Ni(II) azido complex, Fig. 6f (this weak hypochromism was calculated as −3.5 %). The percentages were determined from $(\varepsilon_{DNA} + \varepsilon_{COM} - \varepsilon_{DNA\,-\,COM})/(\varepsilon_{DNA} + \varepsilon_{COM}) \times 100$, where ε_{DNA} is the extinction coefficient of CT-DNA, ε_{COM} is the extinction coefficient of a free Ni(II) complex, and $\varepsilon_{DNA\,-\,COM}$ is the extinction coefficient of a DNA-bound Ni(II) complex.

The weak hypochromic effect was observed for interactions between [Ni**L**(NCS)]BF_4 or [Ni**L**Cl]BF_4 and DNA. Evidence for intercalation is normally hypochromism and red shift. In this case, considering the blue shift and the positive charge on the side chain, electrostatic interaction is the probable mode of binding.

In order to further investigate the binding mode, fluorescent displacement experiments were carried out with two different dyes: Hoechst 33258, a minor groove binder, and ethidium bromide, a typical DNA intercalator. Hoechst 33258 (H) binds strongly and selectively with high affinity to double-stranded B-DNA structure and like other minor groove binders, it recognizes at least four AT base pairs. It binds by combination of hydrogen bonding, van der Waals contacts with the walls of the minor groove, and electrostatic interactions between its cationic structure and the DNA [43]. Binding of Hoechst 33258 to CT-DNA was followed by excitation at 350 nm with maximum in fluorescence at 444 nm. The fluorescence intensity of the band at 444 nm of the Hoechst–CT-DNA system decreased remarkably with the increasing concentrations

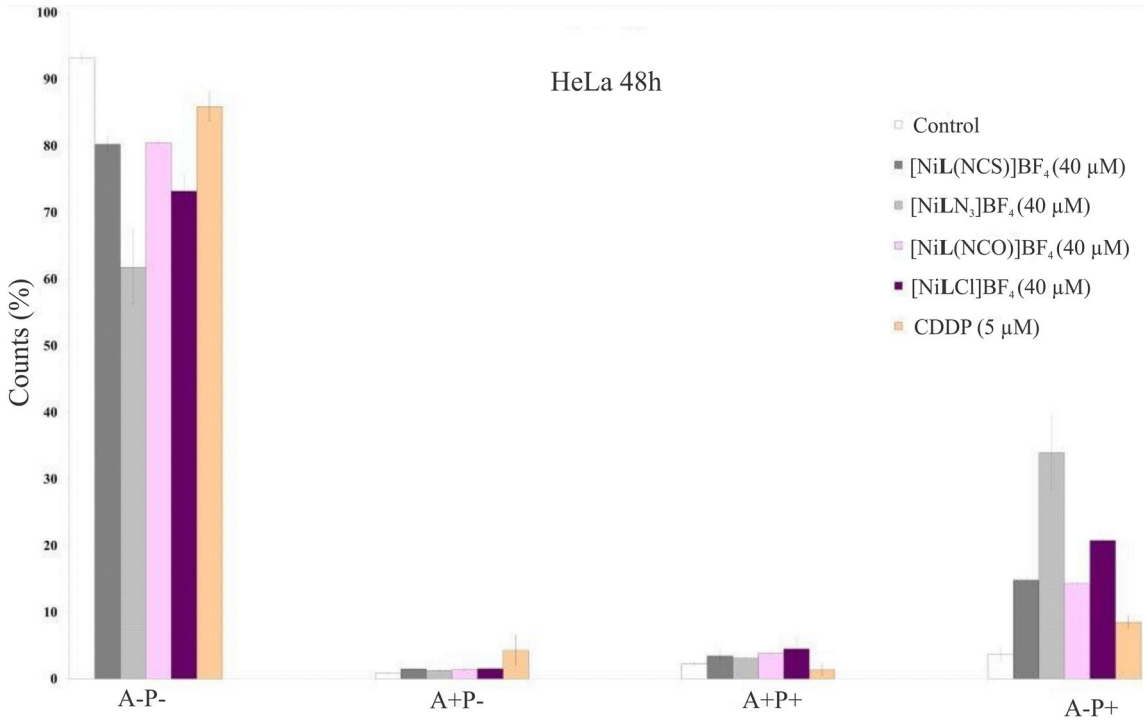

Fig. 5 Bar graphs of percent of HeLa cells labeled with Annexin V-FITC (A) and PI (P) quantified by FACS, after 48 h treatment with nickel(II) complex ([Ni**L**(NCS)]BF_4, [Ni**L**N_3]BF_4, [Ni**L**(NCO)]BF_4 and [NiLCl]BF_4) and CDDP (with 40 μM concentration for nickel(II) complexes and 5 μM concentration for cisplatin); *bar graphs* represent mean ± SD of triplicates of one experiment

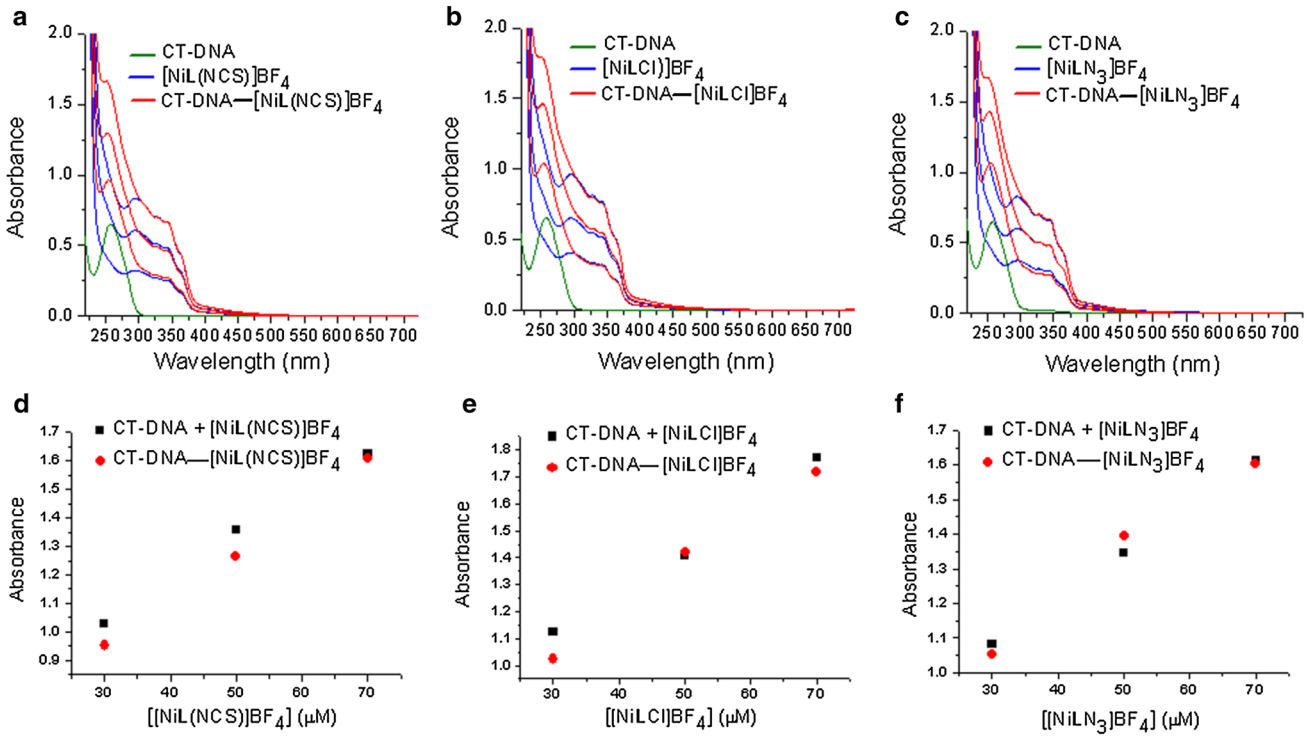

Fig. 6 Changes in UV–Vis absorption spectra of CT-DNA (88 μM) after interaction with different concentrations of Ni(II) complexes. **a–c**: UV–Vis absorption spectra of [Ni**L**(NCS)]BF_4 (30, 50 and 70 μM), [Ni**L**Cl]BF_4 (30, 50 and 70 μM) and [Ni**L**N_3]BF_4 (30, 50 and 70 μM), respectively, before and after interaction with CT-DNA; **c–e** comparison of absorption at 258 nm between the CT-DNA–Ni(II) complexes and the sum values of CT-DNA and Ni(II) complexes

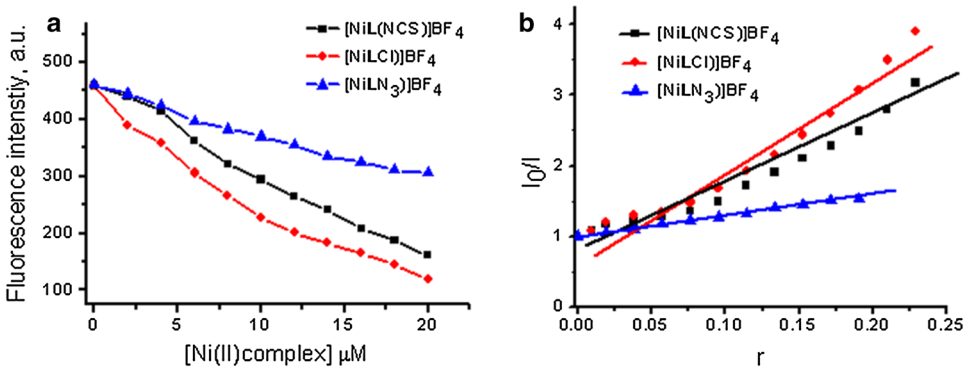

Fig. 7 Displacement of DNA-bound Hoechst 33258 (H) by Ni(II) complexes: **a** changes of fluorescence intensities at $\lambda_{max} = 444$ nm with concentration of the complexes and **b** fluorescence quenching curves of H bound to CT-DNA at $\lambda_{max} = 440$ nm by [Ni**L**(NCS)]BF_4, [Ni**L**Cl]BF_4 and [Ni**L**N_3]BF_4; $\boldsymbol{r}$ = [Ni(II) complex]/[CT-DNA]

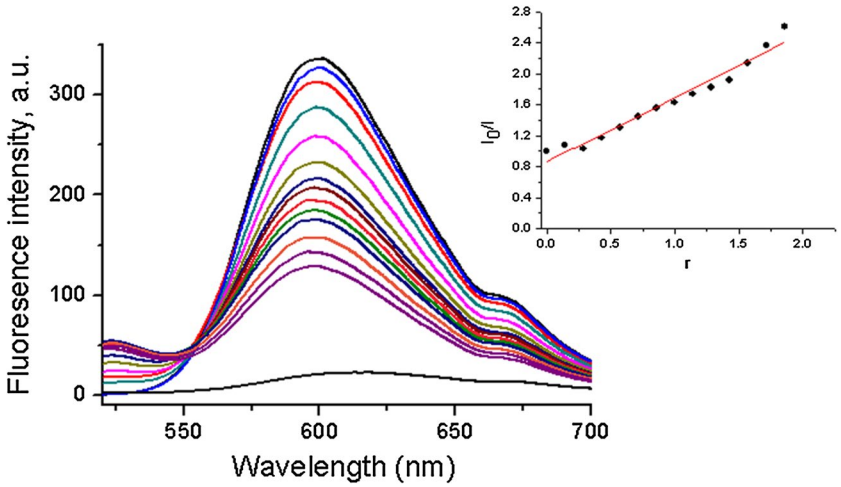

Fig. 8 Displacement of DNA-bound ethidium bromide (EB) by [Ni**L**N_3]BF_4 complex: emission spectra ($\lambda_{ex} = 500$ nm) of EB alone (25 μM, *bottom line*), EB bound to CT-DNA (100 μM, *top line*) and quenching of EB–CT-DNA system by the complex at increasing concentrations (0.5, 1, 1.5, 2, 4, 6, 8, 10, 12, 14, 16, 18 and 20 μM, curves from *top to bottom*); *inset* fluorescence quenching curves of EB bound to CT-DNA at $\lambda_{max} = 600$ nm by [Ni**L**N_3]BF_4; $\boldsymbol{r}$ = [Ni**L**N_3]BF_4]/[CT-DNA]

of the Ni(II) complexes (Fig. 7a). The maximal decrease of fluorescence intensity of Hoechst—CT-DNA by [Ni**L**Cl]BF_4 was 75 %, by [Ni**L**(NCS)]BF_4, 65 % and by [Ni**L**N_3]BF_4 35 %. Results showed that the displacement of Hoechst by [Ni**L**N_3]BF_4 was less efficient than by other two nickel(II) complexes. These results were consistent with quenching curves shown in Fig. 7b that were applied to determine K by linear regression of a plot of I_0/I against $\boldsymbol{r}$. The quenching constants calculated from the Stern–Volmer equation [30] were $K = 10.31$, $K = 15.35$ and $K = 2.88$ for [Ni**L**(NCS)]BF_4, [Ni**L**Cl]BF_4 and [Ni**L**N_3]BF_4, respectively. These data suggest minor groove binding of chlorido and isothiocyanato complexes, but for azido complex, a possible destabilization of DNA structure, especially if hyperchromism (about −3.5 %) occurring in UV spectra at higher concentrations of the complex is taken into account.

For the further study of the binding mode between a Ni(II) complex and DNA, fluorescence quenching of DNA-bound ethidium bromide (EB) system by [Ni**L**(NCS)]BF_4, [Ni**L**Cl]BF_4 and [Ni**L**N_3]BF_4 was investigated. Isothiocyanato and chlorido Ni(II) complexes did not quench the fluorescence of EB under the applied experimental conditions. The result of the displacement experiment using the intercalator ethidium bromide by [Ni**L**N_3]BF_4 complex is shown in Fig. 8. It showed that there was significant reduction (up to 38 %) in the fluorescence intensity of DNA–EB by increasing concentrations of [Ni**L**N_3]BF_4 complex, accompanied by blue shift of emission maximum from 600 to 596 nm, so that an isosbestic point was formed at 550 nm. These changes are typical of metal complex bound to double-stranded DNA through non-covalent interactions [44]. Fluorescence quenching data were analyzed by according to the Stern–Volmer Eq. (1) The value $K = 0.965$ was calculated from the ratio of the slope to the intercept from the plot of I_0/I versus $\boldsymbol{r}$ ($\boldsymbol{r}$ = [Ni**L**N_3]BF_4]/[CT-DNA]), demonstrated in inset in Fig. 8.

DNA cleavage studies

The ability of Ni(II) complexes to cleave double-stranded plasmid DNA were investigated using an agarose electrophoretic assay. The assay allows assessment of DNA strand cleavage by monitoring the conversion of untreated supercoiled form (FI) plasmid DNA into the nicked form (FII) and linear form (FIII). As shown in Fig. 9 (lane P), plasmid pUC19 consisted mainly of FI and FII. An addition of a complex to the plasmid resulted in formation of a linear form FIII and gradual disappearance of supercoiled form

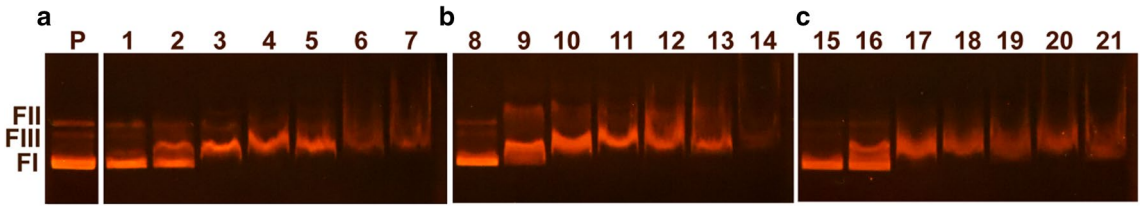

Fig. 9 Agarose gel electrophoretic analysis of plasmid pUC19 (512 ng) without (*lanes P*) and pUC19 (512 ng) with 0.1, 0.2, 0.3. 0.4, 0.5, 0.6 and 0.8 mM complex [Ni**L**(NCS)]BF_4, *lanes 1–7*, respectively—(**a**); pUC19 (512 ng) with 0.1, 0.2, 0.3, 0.4, 0.5, 0.6 and 0.8 mM complex [Ni**L**Cl]BF_4, *lanes 8–14*, respectively—(**b**); pUC19 (512 ng) with 0.1, 0.2, 0.3, 0.4, 0.5, 0.6 and 0.8 mM complex [**NiL**N_3]BF_4, *lanes 15–21*, respectively—(**c**)

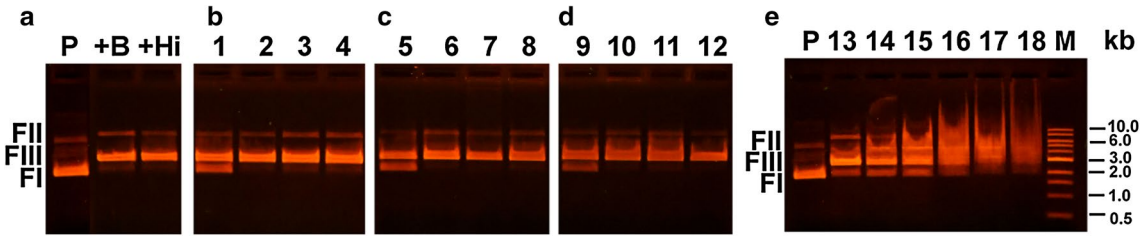

Fig. 10 Agarose gel electrophoretic analysis of restriction endonuclease fragmentation of pUC19 (512 ng) by *Bam*HI (10 U) and *Hin*dIII (10 U) after and before interactions with the Ni(II) complexes: **a** the control samples pUC19—*lane P*, pUC19 digested with *Bam*HI—*lane B*, and pUC19 digested *Hind*III—*lane Hi*; **b** pUC19 after interaction with 0.1 mM [Ni**L**(NCS)]BF_4 digested with *Bam*HI and *Hin*dIII—*lane 1* and *lane 2*, respectively; pUC19 digested with *Bam*HI and *Hind*III before interaction with 0.1 mM [Ni**L**(NCS)]BF_4—*lane 3* and *4*, respectively; **c** pUC19 after interaction with of 0.1 mM [Ni**L**Cl]BF_4 digested with *Bam*HI and *Hind*III—*lane 5* and *lane 6*, respectively, and pUC19 digested with *Bam*HI and *Hind*III before interaction with 0.1 mM [Ni**L**Cl]BF_4—*lane 7* and *8*, respectively; **d** pUC19 after interaction with of 0.1 mM [**NiL**N_3]BF_4, digested with *Bam*HI and *Hind*III—*lane 9* and *lane 10*, respectively; pUC19 digested with *Bam*HI and *Hind*III before interaction with 0.1 mM [**NiL**N_3]BF_4—*lane 11* and *12*, respectively; **e** pUC19 after interaction with increasing concentrations of [Ni**L**N_3]BF_4, complex (0.1, 0.2, 0.3, 0.4, 0.5, and 0.6 mM, *lanes 13–18*, respectively), digested with *Bam*HI; *lane P*—control pUC19; *lane M*—molecular weight markers (1 kb DNA ladder)

in concentration-dependent way (Fig. 9a–c). The generation of the linear form increased gradually up to 0.6 mM of [Ni**L**(NCS)]BF_4 (Fig. 9a, lane 6), up to 0.4 mM of [Ni**L**Cl]BF_4 (Fig. 9b, lane 11) and up to 0.3 mM of [**NiL**N_3]BF_4, (Fig. 9c, lane 17), when the bands of these plasmid forms smeared, indicating that the complexes possess a nuclease activity, converting DNA to shorter fragments. As can be seen in Fig. 9, the electrophoretic patterns indicating nuclease activity were very similar with small differences for all three Ni(II) complexes, the azido complex showing the highest activity.

To check the cleavage activity of Ni(II) complexes, two restriction enzymes were used in reaction with pUC19. Restriction endonucleases typically recognize short (4–8 bp) target sequences, usually palindromic, and cleave double-stranded DNA at specific sites within a

5′ G↓GATCC 3′
3′ CCTAG↑G 5′

and

5′ A↓AGCTT 3′
3′ TTCGA↑A 5′

recognition site [29].

The restriction enzymes *Bam*HI and *Hind*III recognize the sequences: and, respectively, and cut it at position as shown by the arrows.

Restriction enzyme activity is strongly dependent on the local conformation of DNA at the restriction site. Gel electrophoresis revealing the products formed after digestion of plasmid pUC19 by *Bam*HI and *Hin*dIII, in the absence and in the presence of Ni(II) complexes, is shown in Fig. 10. Two bands corresponding to the supercoiled FI and nicked form FII were observed for the undigested plasmid pUC19 (Fig. 10, lane P). After *Bam*HI and *Hin*dIII digestion, the linear forms FIII corresponding to DNA fragment of 3.0 kb were observed (Fig. 10a, lanes B and Hi, respectively). Partial enzyme inhibition of *Bam*HI digestion was observed after the interactions of [Ni**L**(NCS)]BF_4, [Ni**L**Cl]BF_4 and [Ni**L**N_3]BF_4 with pUC19, as shown in Fig. 10b–d, lanes 1, 5 and 9 respectively. When *Bam*HI digestion of plasmid is done first, and then interaction with the complexes followed, there was no further DNA damage by [Ni**L**(NCS)]BF_4 and [Ni**L**Cl]BF_4 (Fig. 10b, c, lanes 2 and 6, respectively). On the contrary, the interaction of [Ni**L**N_3]BF_4 with previously digested DNA produced additional damage at concentration of 0.1 mM, which did not induce damage in pUC19 which had not been exposed to the restriction enzyme, as shown by the smear of the corresponding band (Fig. 10d, lane 10). With increasing concentration

of [Ni**L**N_3]BF_4, more extensive damage was observed (Fig. 10e, lanes 13–18).

*Hind*III activity was not influenced by the presence of [Ni**L**(NCS)]BF_4, and [Ni**L**Cl]BF_4, either before or after interaction with the DNA (Fig. 10b, lanes 3, 4 and Fig. 10c, lanes 7, 8, respectively). The complex [Ni**L**N_3]BF_4 did not inhibit the *Hind*III digestion, as band smear can be seen (Fig. 10d, lane 10), but after the enzyme digestion, the complex did not induce any further damage (Fig. 10d lane 12).

The obtained results indicated that all investigated Ni(II) complexes possess nuclease activity towards supercoiled DNA. They preferentially bind to sequences containing less than four A-T base pairs in double-stranded DNA. Complex [Ni**L**N_3]BF_4 showed a stronger activity than the other two. The observed selectivity of the azido complex for some tumor cell lines can be ascribed to the stronger DNA damaging activity. In comparison to the similar complexes without a positive charge in the side chain [20], the damaging effect was higher, probably due to stronger electrostatic binding. The generally higher cytotoxic activity of the complexes described in this paper compared to those without a positive charge in the side chain [20] could be ascribed to DNA binding and damage.

It should be pointed out that DNA damaging activity cannot be ascribed to simple phosphatase activity of the complexes, since in the experiments with *p*-nitrophenyl phosphate no hydrolysis induced by the complexes could be detected (Fig. S5).

Conclusion

Comparison of cytotoxic activity of Ni(II) complexes with **HL**Cl, **HL1** and **HL2** ligand indicates that the nature of the acylhydrazone and the pseudohalide ligands is important for activity and selectivity of the complexes. Generally, both the 4-phenylsemicarbazone ligand and its Ni(II) complex showed a very high cytotoxic activity, but no selectivity to tumor cell lines. The neutral ester complexes with **HL1** displayed a better selectivity, but a lower activity. The best activity and selectivity were attained with K562 leukemia cells. The positively charged ligand **HL**Cl showed a similar activity as **HL1**, but with selectivity towards lung carcinoma cells A549, which are generally more resistant to chemotherapy. As for the influence of the pseudohalide/halide, in general the most promising are the azido complexes. Regarding possible future applications, the non-electrolyte nature of the Ni(II) complexes with **HL1** and **HL2** ligands might facilitate transport of nickel and pseudohalides through biological membranes, while the presence of positive charge in complexes with **HL**Cl ligand results in enhanced electrostatic interaction with DNA molecule. Metabolic stability of hydrazone ligand (the presence of amide instead of ester group) or similarity with biological molecules (as in the case of Girard's T reagent) might be important properties for enhancement of biological activity. Comparison of biological activity of pseudohalide complexes with the activity of chlorido complex indicates that both monodentate ligand toxicity and its influence on stability of complex compound are responsible for biological activity.

Acknowledgments This work was supported by the Ministry of Education, Science and Technological development of the Republic of Serbia (Grant OI 172055 and Grant III 41026). We thank the Slovenian Research Agency (ARRS) through program P-0175 for financial support and EN-FIST Centre of Excellence, Dunajska 156, 1000 Ljubljana, Slovenia, for using SuperNova diffractometer.

References

1. Kobayashi A, Yamamoto D, Horiki H, Sawaguchi K, Matsumoto T, Nakajima K, Chang H-C, Kato M (2014) Inorg Chem 53:2573–2581. doi:10.1021/ic402879g
2. Jing X, Wu P, Liu X, Yang L, He C, Duan C (2015) New J Chem 39:1051–1059. doi:10.1039/C4NJ01540A
3. Leovac VM, Ribár B, Argay G, Kálmán A, Brčeski I (2006) J Coord Chem 39:11–19. doi:10.1080/00958979608028171
4. Brčeski ID, Leovac VM, Bogdanović GA, Sovilj SP, Revenco M (2004) Inorg Chem Commun 7:253–256. doi:10.1016/j.inoche.2003.11.013
5. Popov LD, Levchenkov SI, Shcherbakov IN, Starikova ZA, Lukov VV, Kogan VA (2014) Russ J Coord Chem 40:280–283. doi:10.1134/S1070328414050108
6. Bacchi A, Carcelli M, Costa M, Fochi A, Monici C, Pelagatti P, Pelizzi C, Pelizzi G, Roca LMSJ (2000) Organomet Chem 593–594:180–191. doi:10.1016/S0022-328X(99)00519-7
7. Pelagatti P, Bacchi A, Carcelli M, Costa M, Frühauf HW, Goubitz K, Pelizzi C, Triclistri M, Vrieze K (2002) Eur J Inorg Chem 439–446. doi:10.1002/1099-0682(20022)2002:2<439::AID-EJIC439>3.0.CO;2-P
8. Pelagatti P, Bacchi A, Balordi M, Bolaño S, Calbiani F, Elviri L, Gonsalvi L, Pelizzi C, Peruzzini M, Rogolino D (2006) Eur J Inorg Chem 2422–2436. doi:10.1002/ejic.200600016
9. Pelagatti P, Bacchi A, Balordi M, Caneschi A, Giannetto M, Pelizzi C, Gonsalvi L, Peruzzini M, Ugozzoli F (2007) Eur J Inorg Chem 162–171. doi:10.1002/ejic.200600731
10. Pelagatti P, Bacchi A, Bobbio C, Carcelli M, Costa M, Fochi A, Pelizzi C (2002) J Chem Soc Dalton Trans 1820–1825. doi:10.1039/B201174N
11. Novaković SB, Bogdanović GA, Brčeski ID, Leovac VM (2009) Acta Crystallogr C 65:263–265. doi:10.1107/S0108270109021970
12. Barandov A, Abram U (2007) Z Anorg Allg Chem 633:1897–1899. doi:10.1002/zaac.200700268
13. Radulović V, Bacchi A, Pelizzi G, Sladić D, Brčeski I, Andjelković K (2006) Monatsh Chem 137:681–691. doi:10.1007/s00706-005-0478-5
14. Malešević N, Srdić T, Radulović S, Sladić D, Radulović V, Brčeski I, Anđelković K (2006) J Inorg Biochem 100:1811–1818. doi:10.1016/j.jinorgbio.2006.07.002
15. Motswainyana WM, Onani MO, Madiehe AM, Saibu M, Thovhogi N, Lalancette RA (2013) J Inorg Biochem 129:112–118. doi:10.1016/j.jinorgbio.2013.09.010

16. Đorđević MM, Jeremić DA, Rodić MV, Simić VS, Brčeski ID, Leovac VM (2014) Polyhedron 68:234–240. doi:10.1016/j.poly.2013.10.029
17. Milenković M, Bacchi A, Cantoni G, Radulović S, Gligorijević N, Aranđelović S, Sladić D, Vujčić M, Mitić D, Anđelković K (2013) Inorg Chim Acta 395:33–43. doi:10.1016/j.ica.2012.09.043
18. Milenković M, Cantoni G, Bacchi A, Spasojević V, Milenković M, Sladić D, Krstić N, Anđelković K (2014) Polyhedron 80:47–52. doi:10.1016/j.poly.2014.01.022
19. Adaila K, Milenković M, Bacchi A, Cantoni G, Swart M, Gruden-Pavlović M, Milenković M, Čobeljić B, Todorović T, Anđelković K (2014) J Coord Chem 67:3633–3648. doi:10.1080/00958972.2014.972389
20. Milenković M, Bacchi A, Cantoni G, Vilipić J, Sladić D, Vujčić M, Gligorijević N, Jovanović K, Radulović S, Anđelković K (2013) Eur J Med Chem 68:111–120. doi:10.1016/j.ejmech.2013.07.039
21. Milenković M, Pevec A, Turel I, Vujčić M, Milenković M, Jovanović K, Gligorijević N, Radulović S, Swart M, Gruden-Pavlović M, Adaila K, Čobeljić B, Anđelković K (2014) Eur J Med Chem 87:284–297. doi:10.1016/j.ejmech.2014.06.079
22. Čobeljić B, Pevec A, Stepanović S, Spasojević V, Milenković M, Turel I, Swart M, Gruden-Pavlović M, Adaila K, Anđelković K (2015) Polyhedron 89:271–279. doi:10.1016/j.poly.2015.01.024
23. Milenković M, Pevec A, Turel I, Milenković M, Čobeljić B, Sladić D, Krstić N, Anđelković K (2015) J Coord Chem. doi:10.1080/00958972.2015.1055260
24. Lever (1984) Inorganic Electronic Spectroscopy, 2nd Ed. Elsevier, Amsterdam pp 534–536
25. Diffraction Oxford (2009) CrysAlis PRO. Oxford Diffraction Ltd., Yarnton
26. Sheldrick GM (2008) Acta Crystallogr A 64:112–123. doi:10.1107/S0108767307043930
27. Supino R (1995) Methods in molecular biology. In: O'Hare S, Atterwill CK (eds) In vitro toxicity testing protocols. Humana Press, New Jersey, pp 137–149
28. Ormerod MG (1994) Analysis of DNA-general methods. In: Ormerod MG (ed) Flow cytometry, a practical approach. Oxford University Press, New York, pp 119–125
29. Sambrook J, Fritsch EF, Maniatis T (1989) Molecular cloning a laboratory manual, 2nd edn. Cold Spring Harbor Laboratory Press, USA
30. Reichmann ME, Rice SA, Thomas CA, Doty P (1954) J Am Chem Soc 76:3047–3053. doi:10.1021/ja01640a067
31. Vijayalakshmi R, Kanthimathi M, Subramanian V (2000) Unni Nair B. Biochem Biophys Res Commun 271:731–734. doi:10.1006/bbrc.2000.2707
32. Sanyal R, Zhang X, Kundu P, Chattopadhyay T, Zhao C, Mautner FA, Das D (2015) Inorg Chem 54:2315–2324. doi:10.1021/ic502937a
33. Nakamoto K (2009) Infrared and Raman spectra of inorganic and coordination compounds, 4th edn. Wiley-Interscience, New York
34. Todorović TR, Rychlewska U, Warżajtis B, Radanović DD, Filipović NR, Pajić IA, Sladić DM, Anđelković KK (2009) Polyhedron 28:2397–2402. doi:10.1016/j.poly.2009.05.002
35. Faqi AS, Richards D, Hauswirth JW, Schroeder R (2008) Regul Toxicol Pharmacol 52:158–162. doi:10.1016/j.yrtph.2008.08.001
36. Koshiishi I, Mamura Y, Imanari T (1997) Biochim Biophys Acta 1336:566–574. doi:10.1016/S0304-4165(97)00073-1
37. Chandler JD, Day BJ (2012) Biochem Pharmacol 84:1381–1387. doi:10.1016/j.bcp.2012.07.029
38. Nazarov AA, Dyson PJ (2011) Metal phosphorus complexes as antitumor agents. In: Peruzzini M, Gonsalvi L (eds) Phosphorus compounds advanced tools in catalysis and material sciences. Springer, Netherlands
39. Savić A, Filipović L, Aranđelović S, Dojčinović B, Radulović S, Sabo TJ, Grgurić-Šipka S (2014) Eur J Med Chem 82:372–384. doi:10.1016/j.ejmech.2014.05.060
40. Kroemer G, Galluzzi L, Vandenabeele P, Abrams J, Alnemri ES, Baehrecke EH, Blagosklonny MV, El-Deiry WS, Golstein P, Green DR, Hengartner M, Knight RA, Kumar S, Lipton SA, Malorni W, Nuñez G, Peter ME, Tschopp J, Yuan J, Piacentini M, Zhivotovsky B, Melino G (2009) Cell Death Differ 16:3–11. doi:10.1038/cdd.2008.150
41. Li XL, Hu YJ, Wang H, Yu BQ, Yue HL (2012) Biomacromolecules 13:873–880. doi:10.1021/bm2017959
42. Szekely J, Gates KS (2006) Chem Res Toxicol 19:117–121. doi:10.1021/tx050197e
43. Kakkar R, Garg R (2002) Suruchi. J Mol Struct (Theochem) 584:37–44. doi:10.1016/S0166-1280(02)00026-X
44. Hirohama T, Kuranuki Y, Ebina E, Sugizaki T, Arii H, Chikira M, Selvi PT, Palaniandavar M (2005) J Inorg Biochem 99:1205–1219. doi:10.1016/j.jinorgbio.2005.02.020